Article

Statistical Modelling of Biosorptive Removal of Hexavalent Chromium Using Dry Raw Biomasses of *Dioscorea rotundata*, *Elaeis guineensis*, *Manihot esculenta*, *Theobroma cacao* and *Zea mays*

Angel Villabona-Ortíz [1], Candelaria Tejada-Tovar [1] and Ángel Darío González-Delgado [2,*]

1   Process Design and Biomass Utilization Research Group (IDAB), Chemical Engineering Department, Universidad de Cartagena, Avenida del Consulado St. 30, Cartagena de Indias 130015, Colombia; avillabonao@unicartagena.edu.co (A.V.-O.); ctejadat@unicartagena.edu.co (C.T.-T.)
2   Nanomaterials and Computer Aided Process Engineering Research Group (NIPAC), Chemical Engineering Department, Universidad de Cartagena, Avenida del Consulado St. 30, Cartagena de Indias 130015, Colombia
*   Correspondence: agonzalezd1@unicartagena.edu.co

Abstract: Hexavalent chromium [Cr (VI)] is a highly toxic and hazardous contaminant that poses serious health risks to both humans and the environment. Its presence in water sources can lead to severe health issues, including various types of cancer and respiratory ailments. Therefore, developing efficient and effective methods for Cr (VI) removal is crucial in ensuring safe and clean water supplies. The aim of this research is the environmentally responsible elimination of hexavalent chromium by bioadsorption using corn residues (CR), palm fiber (PF), and the peels of yam (YP), cassava (CP), and cocoa (CH). The study was conducted with varying levels of pH, bioadsorbent quantity, temperature, and adsorbent particle size at 200 rpm, with an initial concentration of 100 mg/L and 24 h of contact time to improve the adsorption efficiency. The process variables were evaluated and optimized using the statistical technique response surface methodology (RSM). The SEM-EDS analysis revealed that the predominant elements in the structure of the bioadsorbents were carbon and oxygen. Furthermore, the adsorption process led to the incorporation of Cr (VI) into the structure of the biomaterials, as indicated by their EDS spectra. The maximal adsorption efficiency of 99.11% was obtained at pH 2, bioadsorbent dose of 0.03 mg, 30 °C, and 0.5 mm of particle size. Various equilibrium isotherms were utilized to fit and analyze the adsorption data. The assessed maximum adsorption capacities were 38.84, 56.88, 52.82, 138.94, and 240,948.7 mg/g for YP, PF, CP, CH, and CR, respectively. The adsorption data exhibited conformity with the Freundlich and Redlich–Peterson isotherm models (R^2 = 0.95), indicating that the phenomenon occurs in a multilayer. Pseudo-second order and Elovich kinetic models adjusted the kinetics of chromium (VI), suggesting that the mechanism could be controlled by chemisorption. Therefore, the residual biomasses evaluated can serve as a cost-effective adsorbent for Cr (VI) removal, and the use of RSM enables efficient modeling and prediction of the adsorption process.

Keywords: adsorption; Cr (VI); dry biomass; equilibrium; kinetics; response surface methodology

1. Introduction

Chromium exists naturally and can be found in rocks, soil, and water. It appears in two primary forms: Cr (III) and Cr (VI) [1]. While trivalent chromium [Cr (III)] is an essential nutrient for humans, hexavalent chromium [Cr (VI)] is toxic and poses significant health risks since it is classified as a human hazard by the International Agency for Research on Cancer (IARC) [2]. Chromium pollution is a major environmental concern, and its sources include industrial discharges, mining operations, and agricultural practices [3]. Cr (VI) is frequently utilized in diverse industrial sectors, including electroplating, textile

manufacturing, and leather tanning. Improper handling and disposal of Cr (VI) waste can lead to its release into the environment, where it can contaminate soil, water, and air [4]. Contact with Cr (VI) through contaminated water, food, and air can cause lung cancer, nasal and sinus cancer, and cancer of the gastrointestinal tract, as well as respiratory irritation, asthma, allergic dermatitis, liver damage, nausea, vomiting, and diarrhea [5,6]. It has been established that concentrations exceeding 0.05 mg/L of Cr (VI) and 5 mg/L of Cr (III) can have toxic effects on living organisms, and a maximum concentration of chromium total of 100 µg/L is recommended in drinking water by US Environmental Protection Agency (US EPA) [7].

The effective and economical way to eliminate Cr (VI) from contaminated environments is a critical research area. The development of capable and renewable methods for the removal of Cr (VI) is essential to mitigate the health risks associated with exposure to this toxic metal. The process of removing heavy metals using biological materials (bioadsorption) has become an affordable and eco-friendly alternative for eliminating Cr (VI) from polluted water and soil [8]. Thus, research in this area has the potential to provide sustainable solutions for the management of chromium pollution.

Lignocellulosic biomasses have been investigated as probable bioadsorbents for the clearing of heavy metals from wastewater, particularly for the elimination of Cr (VI) from the aqueous medium, including chromium six. The cost-effective, renewable nature and high availability of these biomasses make them an attractive option as adsorbents [9]. Different types of lignocellulosic biomasses have been evaluated as adsorbents for chromium (VI), including agricultural wastes, forestry residues, and aquatic plants [10–12]. Agricultural wastes such as rice husk [13], wheat straw [14], sugarcane bagasse [15], and corn cob [16] have shown promising results as adsorbents for Cr (VI). These materials contain high amounts of cellulose and hemicellulose, which provide attachment points for the metal ions [17]. Forestry residues, such as sawdust and wood chips, are also effective adsorbents for chromium six due to their high surface area and permeability [18].

Taking the above into account, the aim of this article is to explore the bioadsorption of chromium (VI) using dry biomass obtained from corn residues (CR), palm fiber (PF), peels of yam (YP), cassava (CP), and cocoa (CH), which were selected due to the large quantity of post-harvest waste generated as a result of cultivating these species in the Bolivar department (Colombia) [19]. The effect of pH was established, and a central composite experimental design (CCD) was followed to analyze the impact of temperature, particle size, and adsorbent dosage. The influence of the initial concentration and the time was analyzed by adjusting the data to equilibrium and kinetic models.

2. Materials and Methods

2.1. Reagents

Potassium dichromate ($K_2Cr_2O_7$) was used to prepare the synthetic solutions, following the ASTM D1687-17 standard method [20]. The initial pH of the solutions was adjusted until the desired values (2, 4, and 6) were reached by adding 1N HCl or 1N NaOH solutions. The chemical reagents employed in this investigation were produced by Merck. In addition, deionized water was used for all analyses.

2.2. Pretreatment of the Biomasses

Palm fiber (PF) was acquired from Bolivar-Colombia; PF is produced as waste during the process of palm oil extraction. YP, CP CH, and CR were obtained after post-harvest handling. The most suitable biomasses were selected to ensure their effectiveness as adsorbents. Subsequently, the biomasses were washed with distilled water four times to remove impurities. Then, biomasses were dried for 24 h in an oven at 60 °C until constant weight. Subsequently, biomasses were size-reduced using an Oster electric mill and sieved for 10 min, selecting particle sizes of 0.14–0.15, 0.315–0.355, 0.45–0.5, 0.9–1.0, and 1.12–1.18 mm, using the sieves N° 100, 45, 35, 18, and 16, respectively.

2.3. Characterization of Bioadsorbents

The bioadsorbents prepared were characterized through Scanning Electron Microscopy (SEM) and Energy Dispersive X-ray (EDX) analyses to investigate their microstructure and surface chemistry using a TESCAN scanning electron microscope coated with gold, 10 kV voltage, and $500\times$ enlargement. The compositional analysis of the bioadsorbents was performed using the methods shown in Table 1.

Table 1. Methods for the analysis of the composition of the biomasses.

Parameters	Method
Cellulose (%)	Digestion-thermogravimetry
Hemicellulose (%)	Digestion-thermogravimetry
Lignin (%)	Photocolorimetry
Pectin (%)	Acid digestion-thermogravimetry
Carbon (%)	AOAC 949.14
Hydrogen (%)	AOAC 949.14
Nitrogen (%)	AOAC 949.13-Kjeldahl

2.4. Batch Adsorption

2.4.1. Adsorption Essays

The impact of pH on the Cr (VI) removal was initially investigated using values of 2, 4, and 6. The adsorption tests were carried out at the best pH value obtained, using a CCD experimental design with three independent factors: temperature, particle size, and dose of biomass. Specific quantities of bioadsorbent and 100 mL of Cr solution were combined in Erlenmeyer flasks for each adsorption test. The blend was stirred on a rotary shaker at 200 rpm for 24 h, at a concentration of 100 mg/L.

2.4.2. Chromium Analysis

After completion of the essays, the bioadsorbent and supernatant were separated through filtration using a microfiber glass filter. A colorimetric method was used to determine the final Cr (VI) quantity in the liquid [21]. The pink complex resulting from the reaction between the Cr (VI) and 1.5-diphenylcarbazide was measured at 540 nm using distilled water as the blank in a Shimadzu UV-Vis UV 1700 spectrophotometer.

The Cr removal percentage from the solution and the amount of chromium adsorbed by the biomass were determined using Equation (1), which considers the initial concentration (C_i) and final concentration (C_f) of Cr (VI) in each test. The adsorption capacity (q) of Cr (VI) in the bioadsorbent was calculated using Equation (2), which considers the initial and final Cr (VI) amounts in the liquid phase, the volume of the liquid phase (100 mL), and the amount of bioadsorbent used in each test (m). The bioadsorption capacity was reported in mg of Cr (VI)/g of biomass.

$$\%E = \frac{C_i - C_f}{C_i} \times 100 \tag{1}$$

$$q_t = \frac{(C_i - C_f) \times V}{m} \tag{2}$$

2.4.3. Central Composition Design

Table 2 shows the CCD experimental design implemented to investigate the impact of the factors on the uptake of Cr (VI) in the studied bioadsorbents. The design consists of both real and coded variables. The CCD was set in 16 experiments, which were performed at predetermined levels of the variables (as listed in Table 3). To assess the error related to the procedure and analysis, repeated tests were conducted at the central point (0, 0, 0) for the variables under study (essays 5 and 16 in Table 3). The statistical analysis was conducted using Statgraphics Centurion XIX software (Plains, VA, USA).

Table 2. CCD for the Cr (VI) adsorption in the lignocellulosic bioadsorbents under study.

Independent Variable	SCode	Factor Level and Variable Value				
		$-\alpha$	-1	0	$+1$	$+\alpha$
Temperature (°C)	A	30	40	55	70	80
Particle size (mm)	B	0.135	0.355	0.677	1	1.22
Adsorbent dose (g)	C	0.031	0.15	0.325	0.5	0.619

Table 3. Adsorption tests of the CCD.

Test	Temperature, °C	Particle Size, mm	Adsorbent Dose, g
1	40.0	1.0	0.5
2	40.0	1.0	0.15
3	55.0	1.219	0.325
4	55.0	0.6775	0.03
5	55.0	0.6775	0.325
6	70.0	0.355	0.5
7	80.22	0.6775	0.325
8	70.0	0.355	0.15
9	40.0	0.355	0.15
10	70.0	1.0	0.15
11	40.0	0.355	0.5
12	29.77	0.6775	0.325
13	55.0	0.135	0.325
14	70.0	1.0	0.5
15	55.0	0.6775	0.619
16	55.0	0.6775	0.325

2.4.4. Thermodynamic Analysis

A graphical technique derived from the Van 't Hoff equation was employed to calculate the thermodynamic parameters. The determination of these parameters will provide insight into the probability of the adsorption process and the impact of temperature and pH on it. Specifically, this study aimed to estimate the changes in standard Gibbs free energy ($\Delta G°$), standard enthalpy ($\Delta H°$), and standard entropy ($\Delta S°$). Adsorption capacity tests were conducted on the samples, with temperatures ranging from 29 to 81 °C, according to the conditions outlined in the experimental design. Using this information, a graph of $\ln(K_c)$ versus $1/T$ was plotted, and the thermodynamic parameters were estimated [21]. For the estimation of the thermodynamic parameters, Equations (3)–(7) were used, where C_T is the final adsorbate concentration on the surface of the adsorbent in mg/L, and Q_t is the adsorption capacity of the adsorbent in mg/g [22].

$$\Delta G° = -R \times T \times \ln Kc \tag{3}$$

$$\Delta G° = \Delta H° - T \times \Delta S° \tag{4}$$

$$\ln(K_C) = \frac{-\Delta H°}{R \times T} + \frac{\Delta S°}{R} \tag{5}$$

$$K_C = \frac{Q_T}{C_T} \tag{6}$$

2.5. Adsorption Isotherms Study

The isotherm studies were performed using solutions of $K_2Cr_2O_7$ with concentrations from 25 to 500 mg/L and a volume of 100 mL. The essays were made at the best conditions of adsorbent dose, particle size, and temperature obtained after the experimentation fol-

lowing the CCD at 250 rpm. Thereafter, the samples were centrifuged at 10,000 rpm for 10 min, and bioadsorbents were separated from the supernatant; final concentration was determined for the liquid phase. The collected experimental data points were plotted and fitted to non-linear Langmuir, Freundlich, Sips, and Redlich–Peterson adsorption isotherms. The variance, σ^2, was defined according to Equation (7).

$$\sigma^2 = \frac{\sum_{i=1}^{N} \left(y_{i,e} - y_{i,m} \right)^2}{N - p} \tag{7}$$

where $y_{i,e}$ is the experimental data, $y_{i,m}$ is the predicted data by each model, N is the number of data, and *p* is the sum of parameters for each model.

2.6. Adsorption Kinetic Analysis

The reaction rate analysis was carried out under the best conditions obtained for temperature, particle size, and adsorbent dose. Samples were taken at 5, 10, 15, 20, 25, 30, 60, 120, 240, 360, 960, and 1440 min. The estimation of the remaining Cr (VI) was carried out following the procedure presented in Section 2.4.2. The obtained data were fitted to the Lagergren pseudo-first-order, pseudo-second order, Elovich, and intraparticle diffusion kinetic models.

3. Results and Discussion

3.1. Surface Characterization of Bioadsorbents

The morphological and compositional properties of the bioadsorbents were studied, and Figures 1–5 show their characteristics before and after the adsorption process using SEM-EDS. The predominant component of the five bioadsorbents is carbon, which is followed by oxygen. This can be attributed to the lignocellulosic nature of the material [23,24]. Before adsorption, the presence of elements such as Fe, Cu, Ca, Si, and S are noted, which are part of the structure of plants because of their function during photosynthesis, respiration, and synthesis of lignin, enzymes, and proteins [25]. Minerals such as calcium, magnesium, and potassium are necessary for plant growth and development, as they are involved in the formation of cell walls, cell division, and the regulation of water and nutrient uptake [26]. In SEM micrographs before adsorption, the presence of white particles, attributed to metallic cations such as Ca^{2+}, Mg^{2+}, K^+, Si^+, and Fe^+, are observed, which are retained in the active centers of the materials due to the electrostatic attraction of the carboxylic groups. YP, CP, and CH are the bioadsorbents with the most diverse structure, while the structures of CR and PF are less complex, which can be attributed to the agro-industrial utilization of these prior to their disposal and their use as adsorbent material. These results align with our previously reported surface area values of the adsorbents YP (0.946 m^2/g), PF (2.732 m^2/g), CP (2.051 m^2/g) [27], CH (1.45 m^2/g) [28], and CR (0.979 m^2/g) [29].

After the removal process, the formation of complexes on the surface of the bioadsorbents is noted. Regarding the SEM and EDS analyses of the biomaterials, it is observed that after removal, more white granular crystals are formed, which are loaded with Cr (VI); EDS analysis confirms the presence of Cr (VI) ions due to the characteristic high-density peak at 0.573 and 5.411 keV, which appears after the biosorption. These results are consistent with those previously reported by Chen et al. [30] when using powdered activated carbon for the removal of Cr (VI). Hence, the increase in the number of particles that precipitated on the surface of the five bioadsorbents can be explained by the formation of micro-complexes. This happens when the metal is retained in the active centers of the biomaterials as a result of cation exchange [31]. For more clarity, EDS images are shown in Supplementary Files (Supplementary Files: S1–S5).
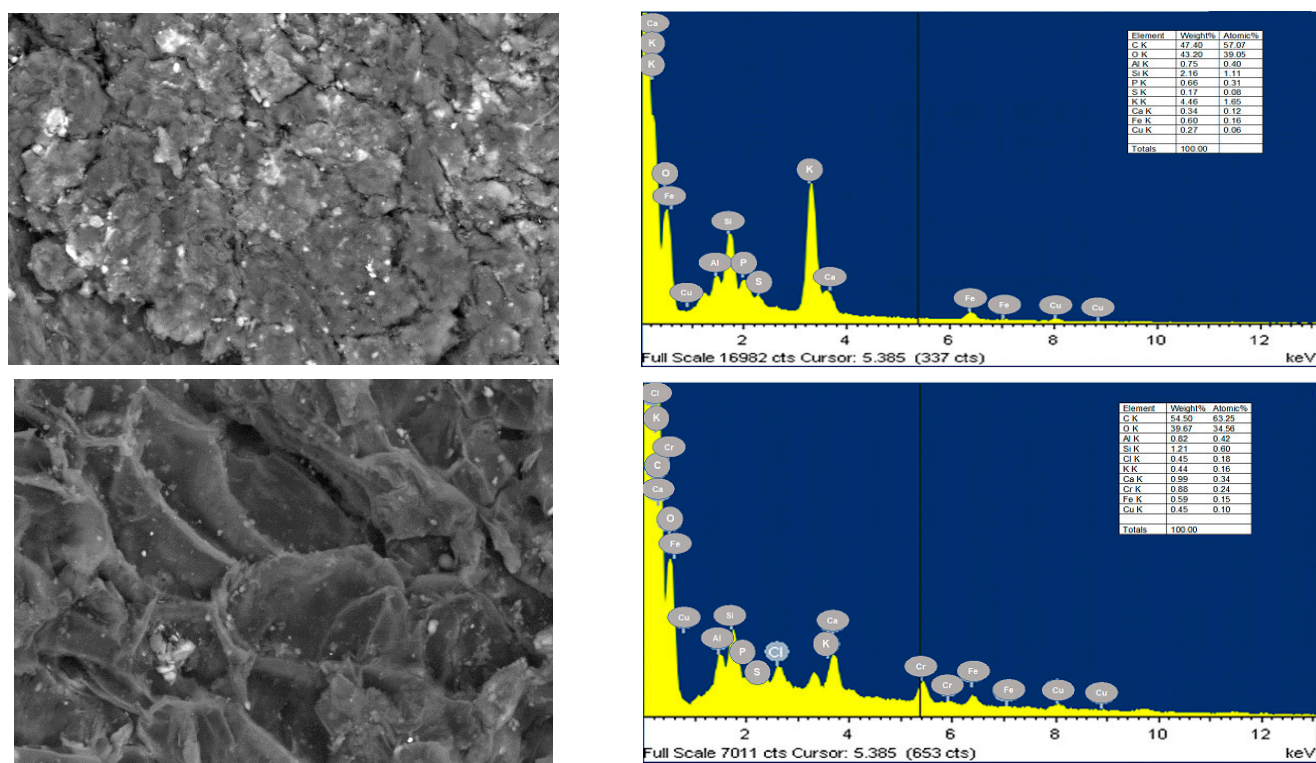
Figure 1. (**Left**) SEM photograph ×500 and (**right**) EDS spectra of YP: (**upper**) before and (**lower**) after Cr (VI) adsorption.
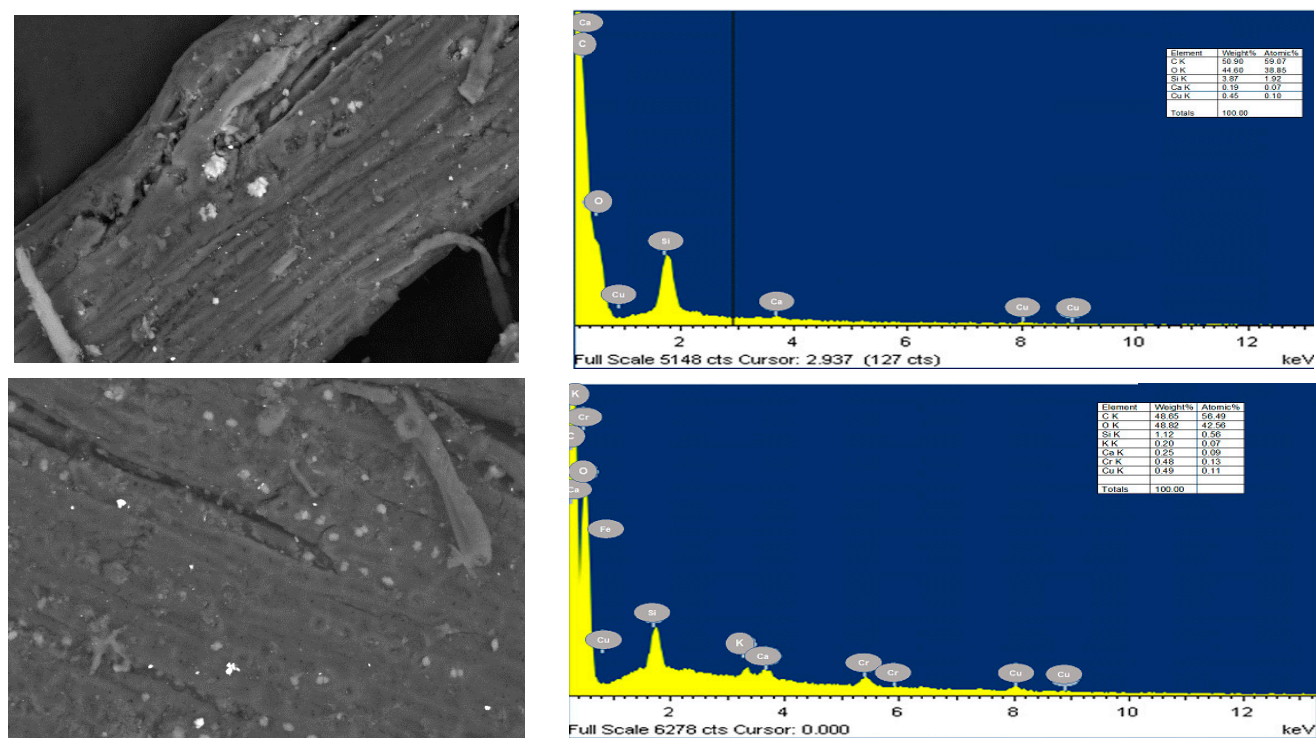

Figure 2. (**Left**) SEM photograph ×500 and (**right**) EDS spectra of PF: (**upper**) before and (**lower**) after Cr (VI) adsorption.
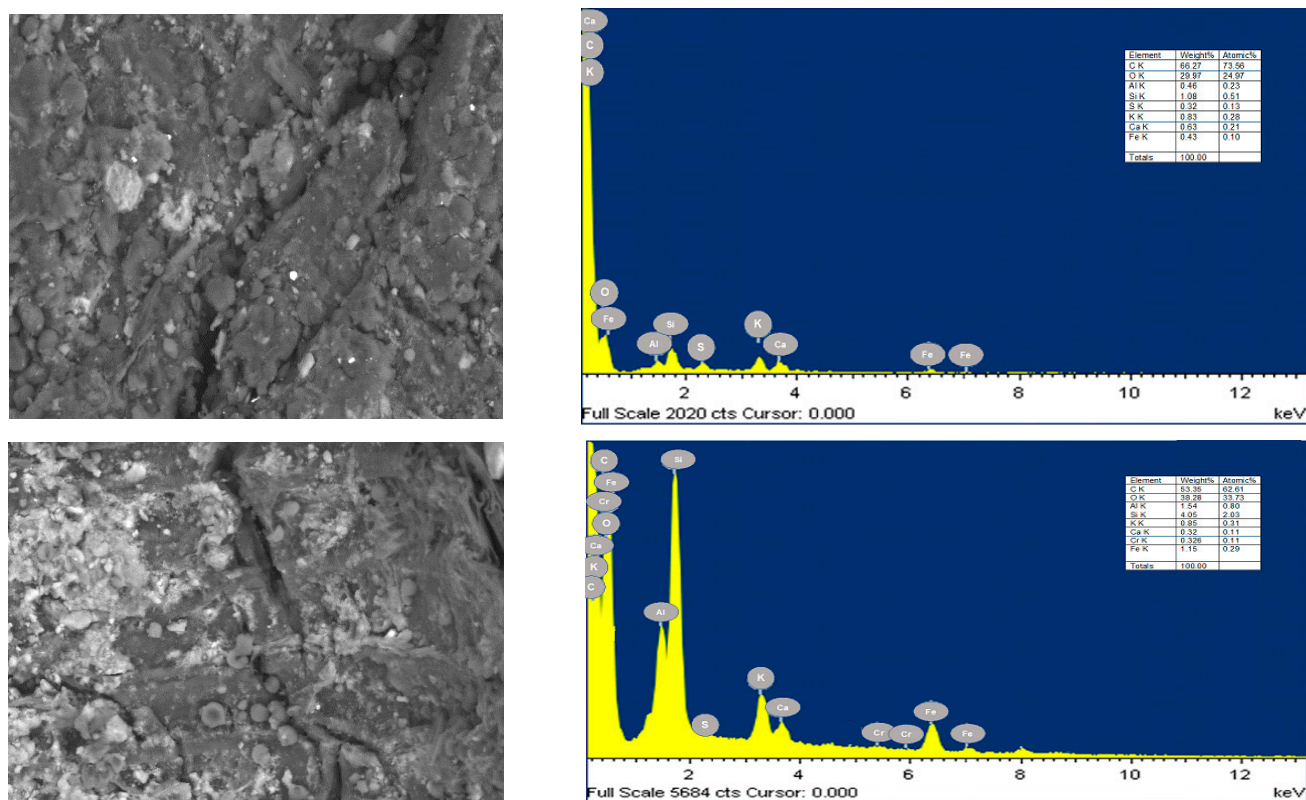
Figure 3. (**Left**) SEM photograph ×500 and (**right**) EDS spectra of CP: (**upper**) before and (**lower**) after Cr (VI) adsorption.
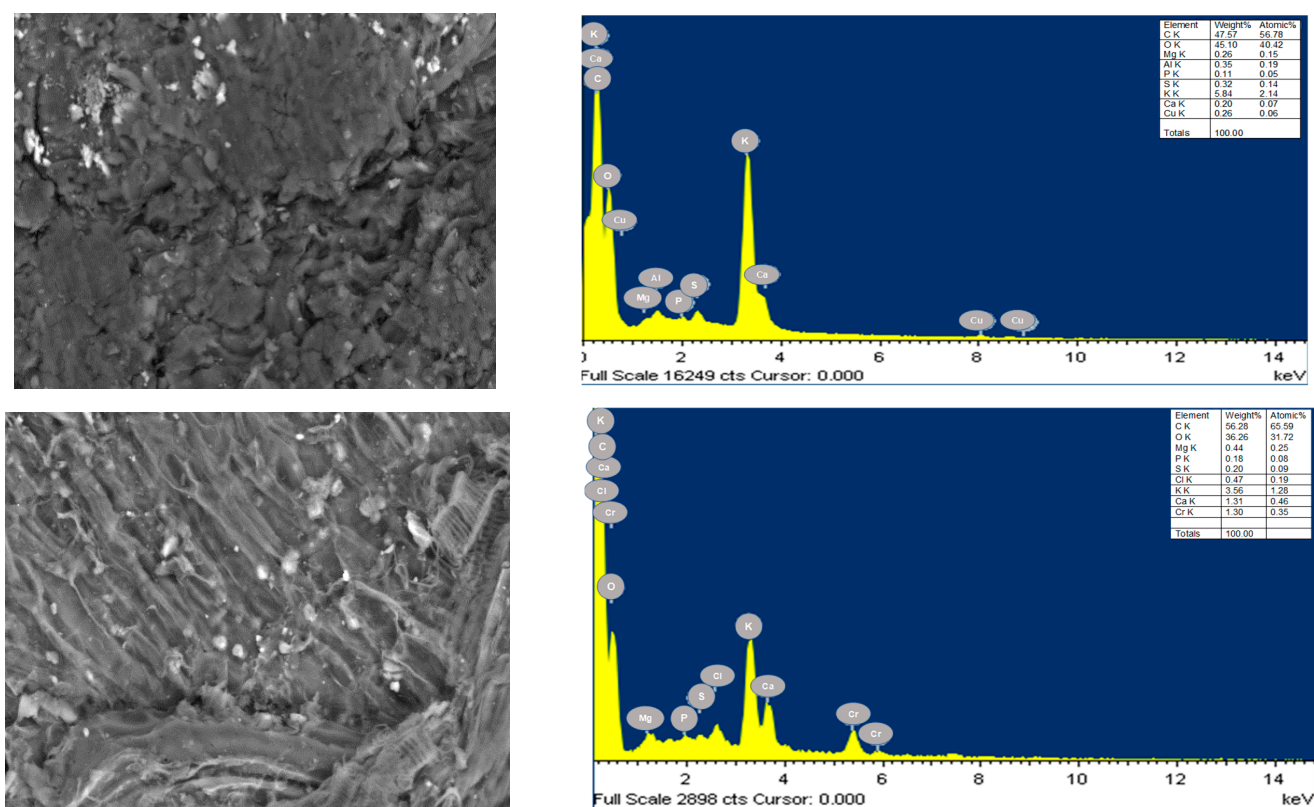

Figure 4. (**Left**) SEM photograph ×500 and (**right**) EDS spectra of CH: (**upper**) before and (**lower**) after Cr (VI) adsorption.
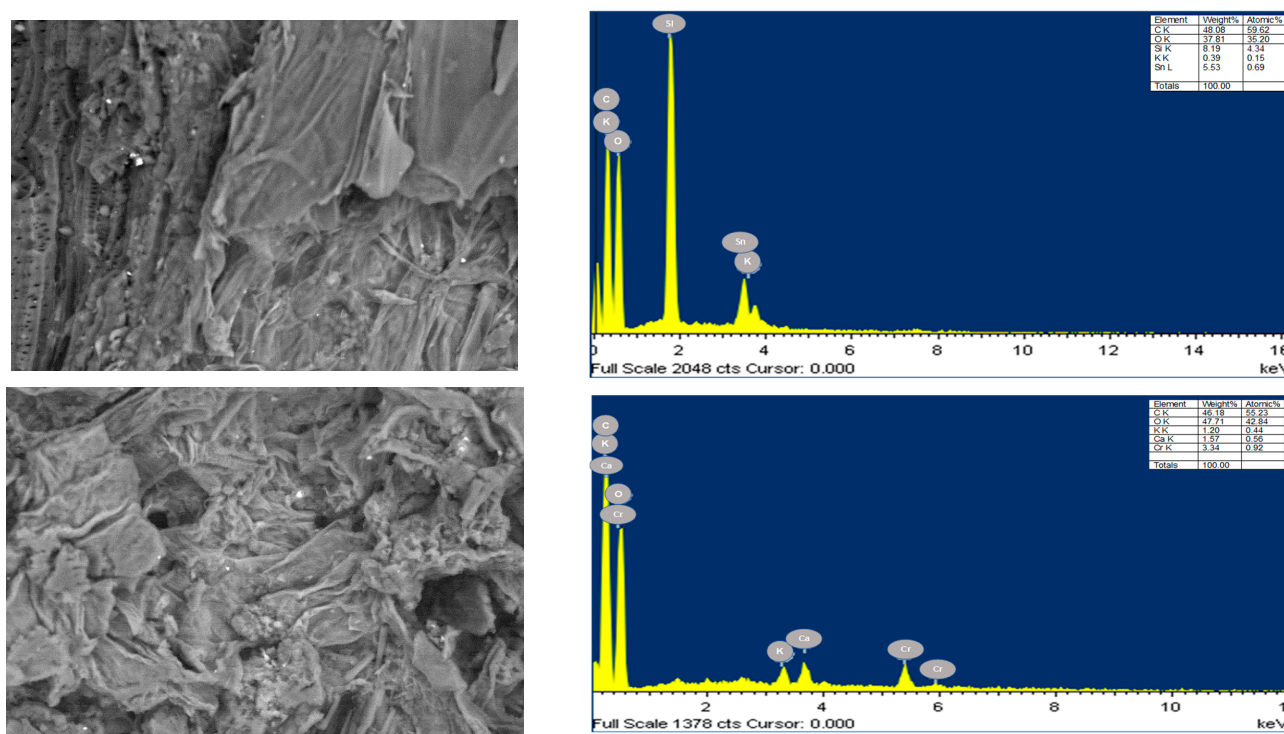
Figure 5. (**Left**) SEM photograph ×500 and (**right**) EDS spectra of CR: (**upper**) before and (**lower**) after Cr (VI) adsorption.

Results from the bromatological analysis shown in Figure 6 confirm that the biomasses are mostly composed of cellulose, and carbon is the main constituent of the biomasses, followed by hydrogen. The above makes the bioadsorbents under study also attractive for their use as a fuel material. In addition, the existence of lignin, cellulose, and hemicellulose in each bioadsorbent has been directly related to a substantial removal effectiveness because these polymers contain numerous hydroxyl groups, and in the case of lignin, phenolic groups, which can promote metal adsorption [32–34]. Likewise, it is observed that YP has a lower presence of lignin compared to the other biomasses, so lower performance is expected in its efficiency as an adsorbent of Cr (VI) ions. Biomass has the capability to adsorb Cr (VI) through several mechanisms, including micro-precipitation, ion exchange, coordination, and complexation. The existence of OH^-, COOH, and amide reactive groups in lignocellulosic materials facilitates these mechanisms, which have been previously reported for the biomasses under study [35]. Nonetheless, the research mentioned the importance of cation exchange and microprecipitation mechanisms in the process by the assessed bioadsorbents.

3.2. Effect of the pH

The pH of the solution has a significant impact on the bioadsorption capacity, mainly due to the phenomenon of protonation that occurs at low pH values and its effect on the chemistry of the solutions [36]; therefore, the adsorption capacity can be influenced by the pH [37]. The binding sites in bioadsorbents are carboxyl, amine, phosphate, sulfate, and hydroxyl groups; the rise in the disposal of these binding sites depends on the displacement of protons, which is pH-dependent [38].
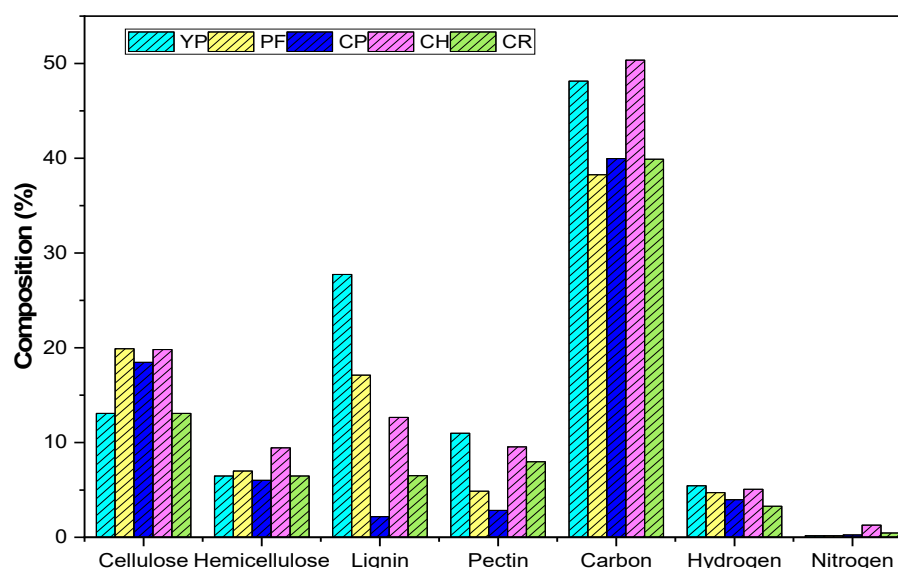
Figure 6. Characterization of bioadsorbents on a wet basis. The deviation of the data is $+/-0.01$.

In Figure 7, the influence of pH on the removal of Cr (VI) is presented with an average deviation of the data of 0.0138 and 0.0251 for the five bioadsorbents under study. In all cases, the best adsorption was observed under a pH of 2. According to the speciation diagram of Cr (VI) [39], it is found that adsorption increases as the pH decreases since the stability of the ionic species of chromium $HCrO_4^-$, $Cr_2O_7^{2-}$, and CrO_4^{2-} highly depends on the pH value. At lower pH values, the active sites of the adsorbents are protonated, and then, anionic species can be linked to the adsorbent due to electrostatic forces. On the other hand, the dominant form of Cr (VI) between pH 1 and 4 is $HCrO_4^-$ [40], so this is the one that is mainly accommodated on the surface of the adsorbent. At higher pH values, the concentration of OH- ions increases, inducing changes in the surface of the adsorbent and preventing the adsorption of Cr (VI) ions.
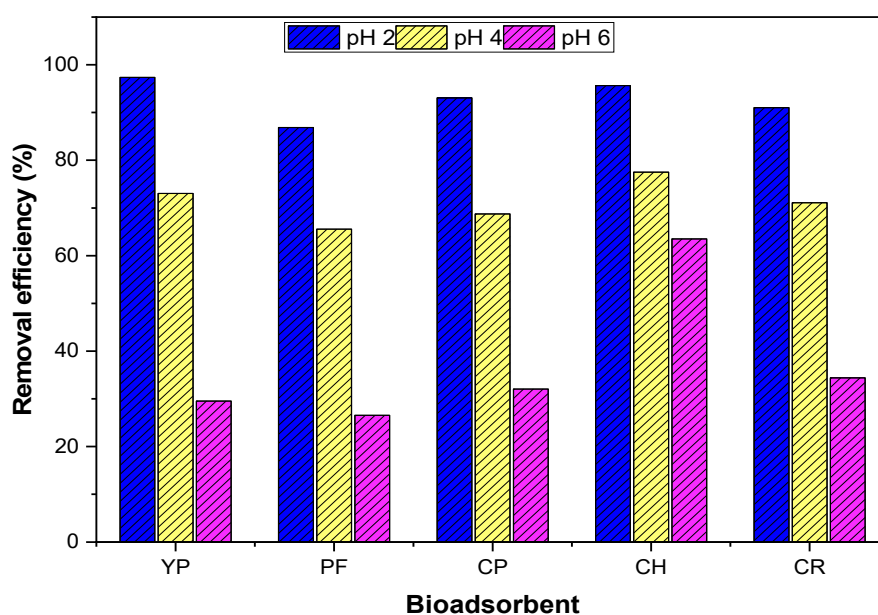

Figure 7. Effect of the pH on Cr (VI) adsorption of bioadsorbents at room temperature, 250 rpm, and 24 h of contact time.

The implementation of an acidic pH level, such as 2, on an industrial scale appears to be impractical due to the large volumes involved. However, the authors are currently

exploring an alternative approach that involves combining different wastewater treatment technologies. This consideration stems from the fact that industrial effluents contaminated with chromium, such as those from tanneries, typically exhibit pH ranges between 3 and 5.5 [41,42]. Within this range, the use of various bioadsorbents has demonstrated a removal efficiency of over 70% (as shown in Figure 7). Therefore, technologies such as electrocoagulation or advanced oxidation technologies, despite being more expensive, exhibit excellent performance when dealing with low concentrations.

3.3. Optimization of Cr (VI) Adsorption by RSM

Table 4 shows the results of the CCD experiments for Cr (VI) removal by the adsorbents under study. The adsorbed amount of Cr (VI) was determined by utilizing Equations (1) and (2) after the adsorption essays to determine the residual Cr (VI) in the aqueous solution. Different statistical designs can assist in evaluating the impact of factors and determining their optimal values for the elimination of Cr (VI) [43]. Based on the surface response method, a model was created based on the experimental data presented in Table 4, which established the trend within a range of 33.70–99.70% (as shown in Table 5). Other studies have also investigated the removal of chromium using waste tires [44], orange peel [45], and Teff husk-based activated carbon, wherein the removal percentages were 79.6%, 97%, and 95.597%, respectively. The results of the removal efficiency of Cr (VI) in terms of coded variables (Table 1) were presented as polynomial equations for each bioadsorbent (Table 5). The coefficients indicate the influence of each factor on the equation, and their signs indicate whether the contribution is positive or negative.

Table 4. CCD experimental design and its response for Cr (VI) removal using palm fibrillates, peels of yam, cassava and cocoa, and corn residues.

| Run | Adsorption Process Variables | | | Cr (VI) Removal, % | | | | | | | | | |
| | | | | PF | | YP | | CP | | CH | | CR | |
	A	B	C	E	RSMP	E	RSMP	E	RSMP	E	RSMP	E	RSMP
1	40.0	1.0	0.5	99.999	100	90.085	100	91.782	100	99.751	100	98.638	100
2	40.0	1.0	0.15	96.541	87.773	51.315	74.412	53.578	67.71	79.662	72.936	81.752	75.556
3	55.0	1.219	0.325	99.999	100	99.999	49.294	98.789	68.709	99.011	100	98.152	100
4	55.0	0.6775	0.03	47.931	67.213	97.763	78.549	96.432	77.424	34.033	51.822	38.782	55.872
5	55.0	0.6775	0.325	95.851	95.008	95.805	97.124	96.456	96.978	99.490	99.041	98.723	97.946
6	70.0	0.355	0.5	99.999	100	99.999	96.495	98.984	89.088	99.491	100	98.764	99.428
7	80.22	0.6775	0.325	99.999	100	99.999	80.787	99.897	96.827	99.032	100	98.153	100
8	70.0	0.355	0.15	99.999	90.549	99.999	96.495	99.474	90.814	99.363	80.609	97.465	88.271
9	40.0	0.355	0.15	99.999	90.009	57.544	45.095	56.456	59.913	79.410	75.758	82.723	75.009
10	70.0	1.0	0.15	99.999	90.009	23.732	57.489	46.156	72.535	99.362	88.717	99.536	89.144
11	40.0	0.355	0.5	99.999	100	99.999	76.938	99.897	77.754	100	100	98.763	100
12	29.77	0.6775	0.325	99.999	100	81.949	86.042	86.156	83.235	99.021	98.191	97.003	97.541
13	55.0	0.135	0.325	99.999	100	23.224	59.933	37.156	61.327	99.013	100	98.153	100
14	70.0	1.0	0.5	99.999	100	23.478	46.622	89.156	89.936	99.362	100	96.248	98.429
15	55.0	0.6775	0.619	98.806	89.265	92.199	96.249	94.156	98.07	99.031	89.001	97.325	87.939
16	55.0	0.6775	0.325	95.852	95.009	95.805	97.103	96.473	96.978	99.012	98.565	98.512	97.946

E is the experimental data, and RSMP is the predicted results by Response Surface Method.

Table 5. Statistical analysis of experimental data for determining optimal conditions.

Biomass	Equation	
PF	$Y = 126.686 - 1.70139A - 53.7905B + 166.658C + 0.0155568A^2$ $+0.0893539AB - 0.164667AC + 33.6544B^2 + 7.65891BC - 193.144C^2$	(8)
YP	$Y = -247.68 + 5.91523A + 386.304B + 321.945C - 0.0215131A^2 - 3.53087AB$ $-3.87998AC - 146.353B^2 - 8.72738BC - 111.798C^2$	(9)
CP	$Y = -92.2692 + 2.9888A + 200.686B + 130.56C - 0.0109166A^2$ $-1.34762AB - 1.86357AC - 108.783B^2 + 84.7243BC - 54.0263C^2$	(10)
CH	$Y = 26.317 + 0.0591254A - 19.6269B + 380.75C + 0.00691135A^2$ $-0.00361757AB - 1.93143AC + 14.9515B^2 - 1.4175BC - 324.249C^2$	(11)
CR	$Y = 32.6509 + 0.0729527A - 17.5524B + 346.157C + 0.00556871A^2$ $+0.0168217AB - 1.66262AC + 13.9998B^2 - 8.28571BC - 299.935C^2$	(12)

where Y is chromium efficiency removal (%) and A, B, and C denotes values of temperature (°C), particle size (mm), and adsorbent dose (g), respectively.

In order to ensure a good adjustment, the regression equation and statistical parameters underwent significance testing through ANOVA [46] from the data presented in Table 4, and the results are summarized in Supplementary Files (Supplementary Files: S1–S5). The significance of the coefficients and model terms were evaluated based on their p-values at a confidence level of 95%. Typically, model terms are considered significant if their p-value is less than 0.05. From ANOVA, it can be said that the bioadsorbent dose (factor C) is the variable with the stronger influence when using CH and CR as Cr (VI) bioadsorbents. When the bioadsorbents are PF, YP, and CP, there is no significant evidence of the influence of the variables in the evaluated range. Overall, it can be concluded that the adsorption percentage of Cr (VI) over CH and CR is favored at a higher bioadsorbent quantity with a low influence of temperature and particle size. Figure 8 shows the normal distribution of residuals for the data, with a single outlier falling outside the range of residuals without transforming the response variable, which affects the accuracy of the equation (left). Additionally, the trend of externally standardized residuals plotted against predicted removal efficiencies is shown on the right of the figure. The plots suggest that the model's predictions and residual precision do not follow any discernible pattern, as indicated by the distance line at zero, confirming the randomness of the residuals.

The equations in Table 5 can be utilized to anticipate the adsorption removal efficiency of Cr (VI) in the tested bioadsorbents within the chosen experimental scope. The visual depiction of the equations is provided in Figure 9. It is observed that at 30 °C, pH 2, and 24 h of contact time, the adsorption removal percentage is higher when the particle size decreases, and the evaluated mean value of the adsorbent dose is employed.

3.4. Thermodynamic Study

For determining the spontaneity and the influence of the temperature on the adsorption for each of the systems evaluated, the values of adsorption entropy ($\Delta S°$), adsorption enthalpy ($\Delta H°$), and Gibbs free energy ($\Delta G°$) were obtained by calculating the adsorption capacity and equilibrium constants (K_C). To achieve this, the Van 't Hoff approach was utilized, which relates the alteration in free energy to the variation in enthalpy and adsorption entropy at different temperatures. This enabled us to determine the regression line of $-\Delta S°$ and obtain $\Delta H°$ through intercepting, as shown in the equation [47]. Results are shown in Table 6.
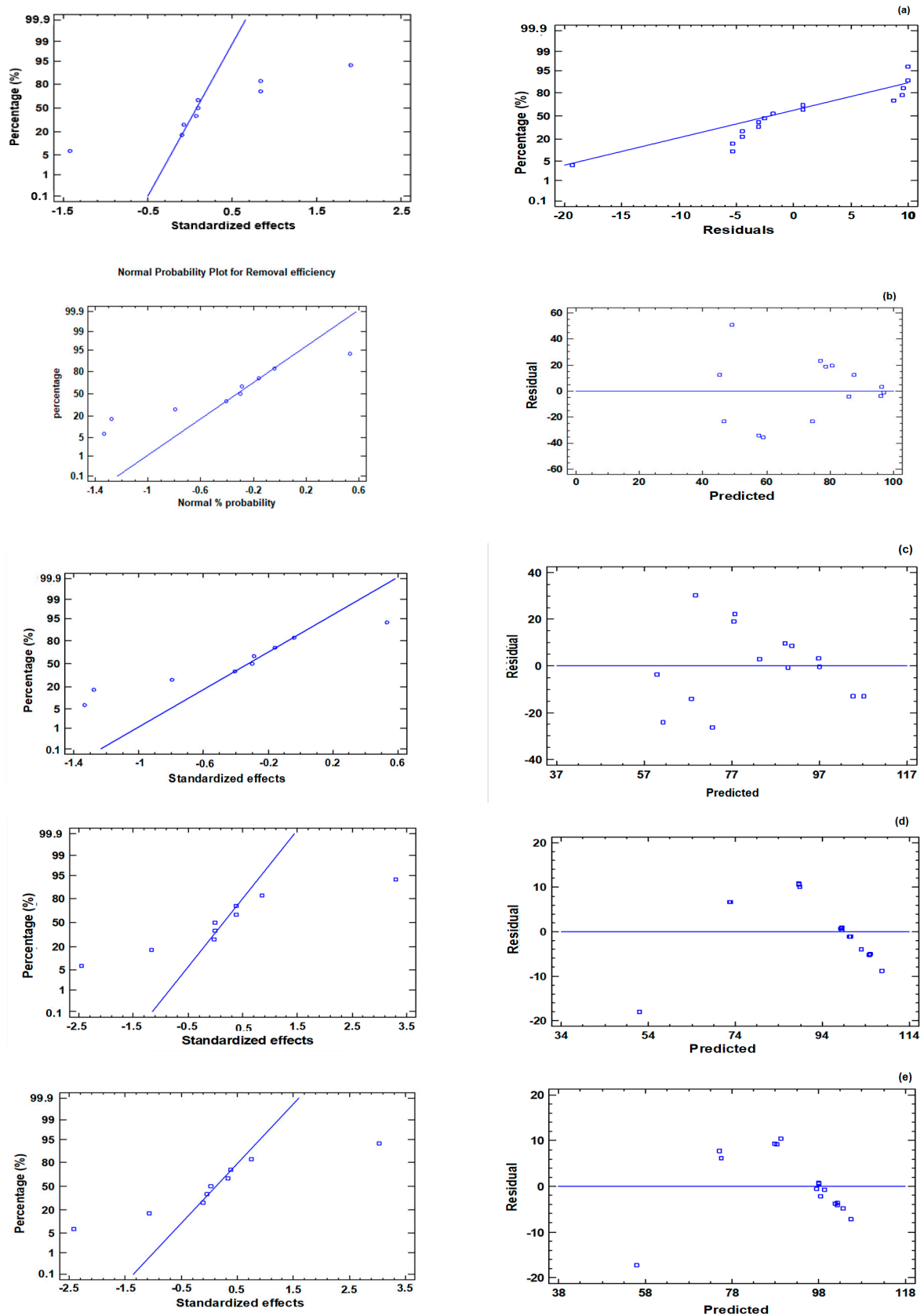
Figure 8. Analytic plots: (**left**) normal probability plot of the residuals and (**right**) externally studentized residuals plot for Cr (VI) removal using (**a**) PF, (**b**) YP, (**c**) CP, (**d**) CH, and (**e**) CR.
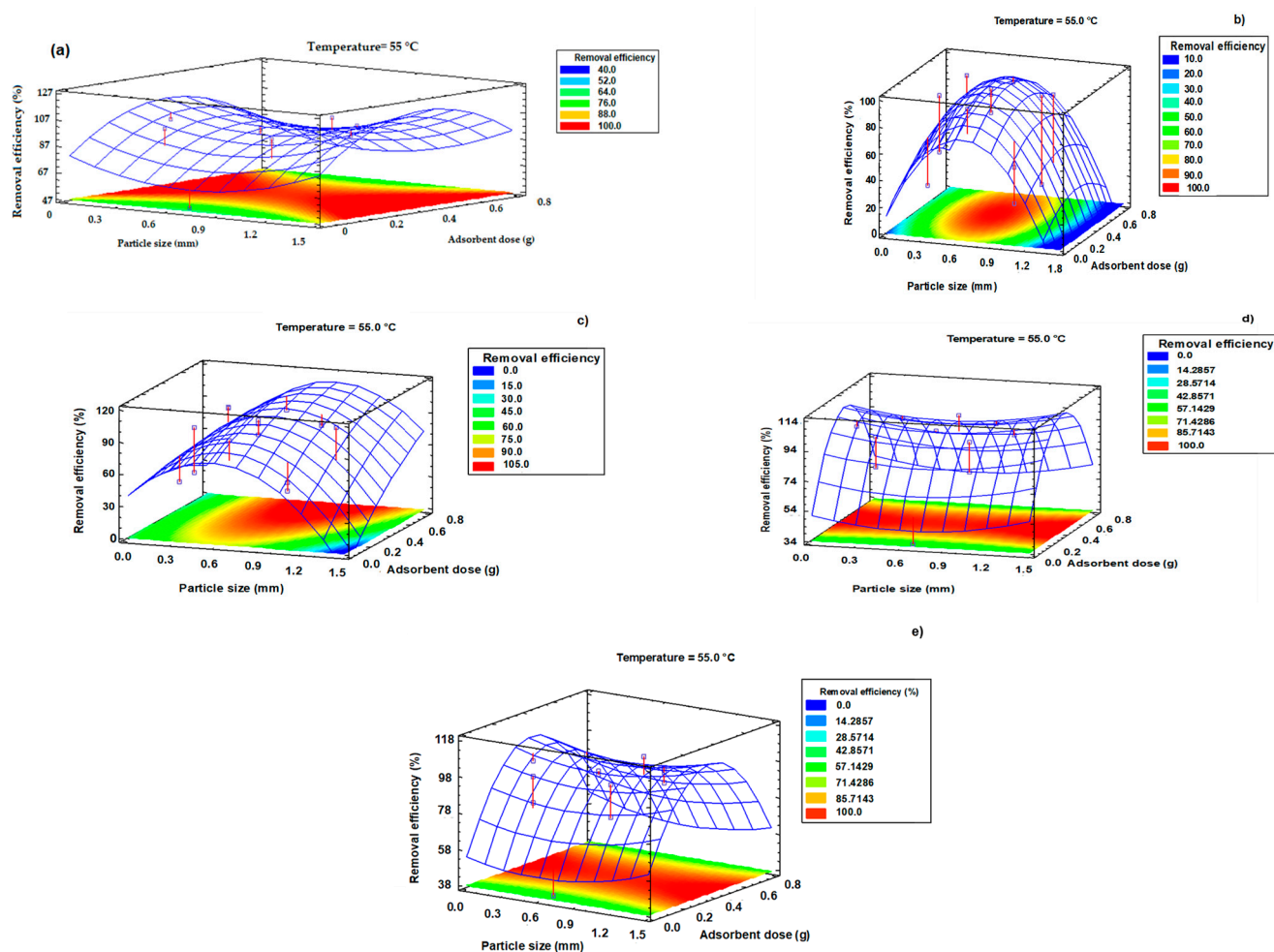
Figure 9. Response surface plots of Cr (VI) efficiency removal % as a function of temperature, particle size, adsorbent dose, and its interaction effects for Cr (VI) removal using (**a**) PF, (**b**) YP, (**c**) CP, (**d**) CH, and (**e**) CR.

Based on these thermodynamic findings, it can be inferred that energy needs to be provided to the system, given the endothermic nature of the process of removing Cr (VI) using YP, CR, and CP bioadsorbents. This is supported by the positive and increasing values of $\Delta H°$ [48,49]; however, data in Table 6 indicate that the ions exhibit higher adsorption efficiency at intermediate and low temperature values. The adsorption process using PF and CH is suggested to be exothermic based on the negative values of enthalpy. This indicates that the system releases energy, resulting in potential energy frugality when scaling up the process [47,50]. A different behavior for the bioadsorbents based on the sign of $\Delta H°$ is observed, thus, might be related to the origin of the biomasses; for example, PF is a residue of the oil palm industry, and it was previously treated with chemicals such as NaOH; meanwhile, the husk and peels (CH, CP, CR, and YP) are agro-residues. The level of processing and degradation of each biomass are different, and this was evidenced in the SEM-EDS shown in Figures 1–5. The above will influence the adsorbate–adsorbent interactions.

The negative values of $\Delta S°$ observed for YP, PF, CP, and CR suggest a strong binding between Cr (VI) and the active centers in the biomass, indicating high affinity and selectivity of the biosorbents towards the metal ion. Additionally, the low randomness at the interface suggests a low possibility of reversibility, resulting in an energetically stable adsorption process [51,52], and the biomass could be inactivated by thermal or physical methods with a low possibility of desorption of the heavy metal, resulting in the immobilization of the pollutant. Cr (VI) has been previously immobilized in orange peel as part of brick matrices, resulting in a release of the metallic ion between 0.21 and 0.25 mg/L after acid

treatments under constant agitation conditions for 18 h [53]. Concentrations below the environmental limit have been reported for Pb (II) and Ni (II) when yam peels are used as bioadsorbents in conjunction with cement-based solidification/stabilization techniques [54]. Successful immobilization of heavy metals through thermal treatment has been reported by incinerating dredged sediments functionalized with phosphate at 700 °C [55]. The low leaching of heavy metals using immobilization techniques is justified by their conversion into more evenly distributed and less soluble metal-bearing phases, reducing their toxic potential [56].

Table 6. Thermodynamic parameters for adsorption of Cr (VI) in the bioadsorbents under study.

YP			
T (K)	**ΔG (kJ/mol)**	**ΔH (kJ/mol)**	**ΔS (kJ/mol·k)**
306.9	1.439	0.057	−0.0465
328.2	2.611		
349.4	3.783		
PF			
T (K)	**ΔG (kJ/mol)**	**ΔH (kJ/mol)**	**ΔS (kJ/mol·k)**
306.9	−0.549	−2.121	−0.143
328.2	0.782		
349.4	12.837		
CP			
T (K)	**ΔG (kJ/mol)**	**ΔH (kJ/mol)**	**ΔS (kJ/mol·k)**
306.9	1.216	0.727	−0.186
328.2	2.341		
349.4	5.876		
CH			
T (K)	**ΔG (kJ/mol)**	**ΔH (kJ/mol)**	**ΔS (kJ/mol·k)**
306.9	2.468	−1.908	−0.354
328.2	4.397		
349.4	13.465		
CR			
T (K)	**ΔG (kJ/mol)**	**ΔH (kJ/mol)**	**ΔS (kJ/mol·k)**
298	1.246	46.772	0.153
323	−2.572		
348	−6.391		

For all the evaluated temperatures, it was observed that when using CR, ΔG° is negative, indicating that the process of adsorption occurs spontaneously, is feasible, and is advantageous. The increase in Gibbs free energy in temperature suggests that spontaneity behaves inversely proportional to the temperature [47,48,50]. Alternatively, when using YP, PF, CP, and CH, ΔG° is positive and rises with increasing temperature, suggesting a decrease in spontaneity and an unfavorable characteristic of the process [11]. As the temperature increases, the magnitude of ΔG° also increases, indicating that the system evolves spontaneously and becomes more favorable for the removal process.

3.5. Effect of the Contact Time

Figures 10–14 show the fitting of the pseudo-first order, pseudo-second order, Elovich, and intraparticle diffusion models of Cr (VI) adsorption kinetics in the five assessed bioadsorbents, respectively. The results indicate that rapid adsorption happens within the first 40 min of the process, with equilibrium being achieved after 90 to 150 min of contact between the ion and the adsorbent. The rapid adsorption observed initially during the

removal process is ascribed to the presence of unoccupied active sites on the surface of the bioadsorbent, which are gradually filled by the ions as time progresses [57].
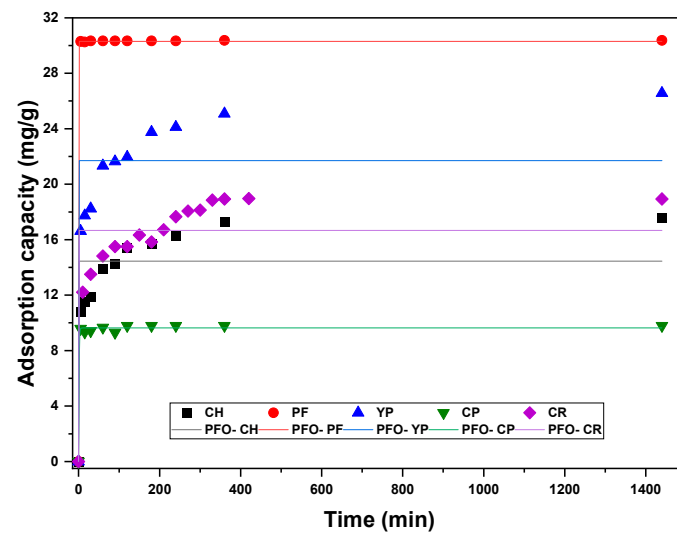

Figure 10. Adjustment of the Cr (VI) adsorption data to the pseudo-first order (PFO) kinetic model.
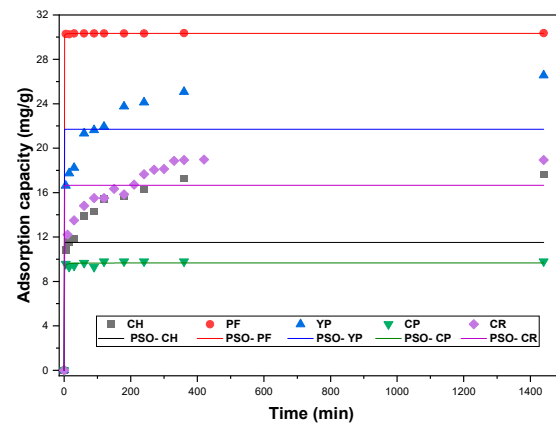

Figure 11. Adjustment of the Cr (VI) adsorption data to the pseudo-second order (PSO) kinetic model.
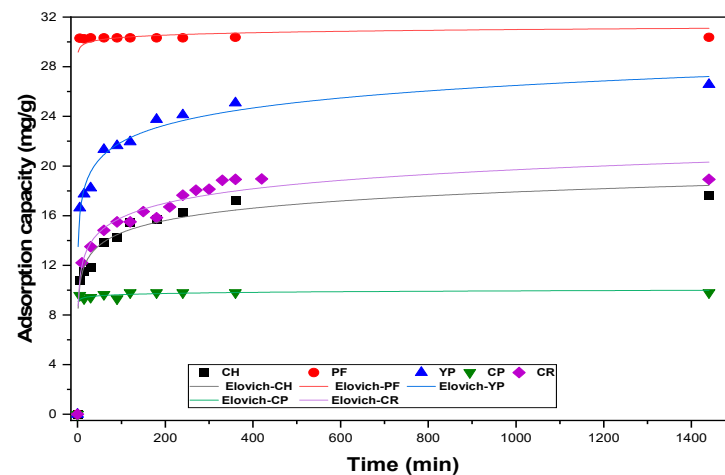

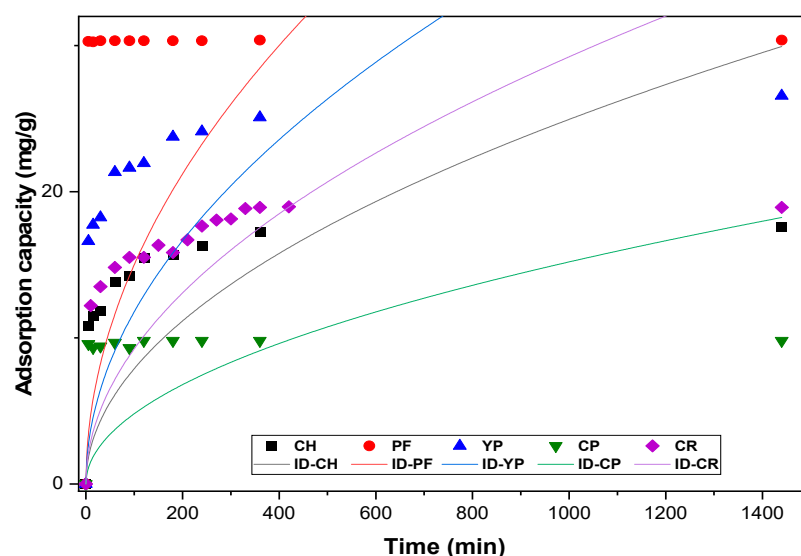**Figure 12.** Adjustment of the Cr (VI) adsorption data to Elovich's kinetic model.

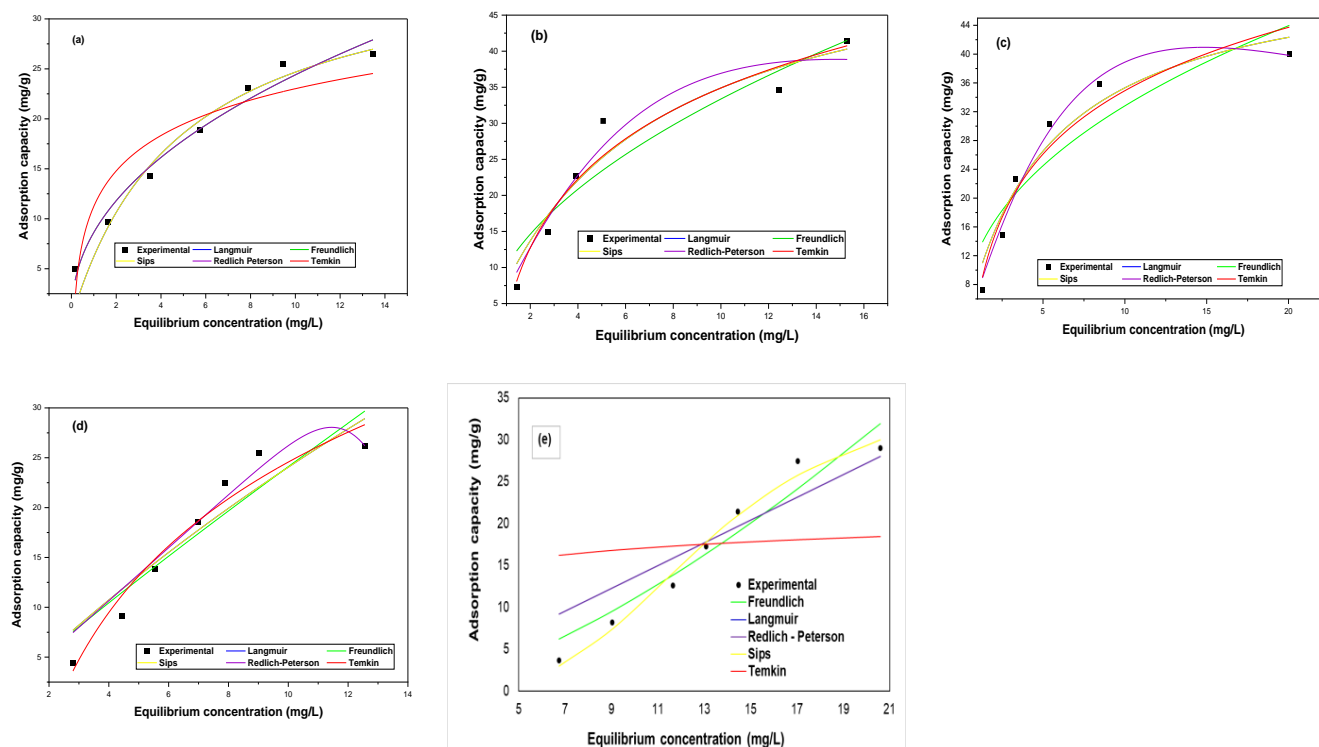**Figure 13.** Adjustment of the Cr (VI) adsorption data to the Intraparticle Diffusion (ID) kinetic model.

Figure 14. Adjustment of the Cr (VI) adsorption equilibrium data of the bioadsorbents from (**a**) YP, (**b**) PF, (**c**) CP, (**d**) CH, and (**e**) CR to the isotherm models.

Based on Figure 10 and Table 7, the pseudo-first order kinetic model is the most appropriate for describing the kinetic data of Cr (VI) removal by CP and PF. This suggests that the rate of adsorption at the surface of the adsorbent is mainly influenced by the disposal of active sites on the adsorbent [58]. The high correlation coefficient (R^2) and low residual errors between the experimental data and the model prediction further support the validity of the model. A similar result was found when using mosambi peel at pH 2, 5 g/L of adsorbent dose, and 125 rpm [59]. Mondal et al. [60] reported that the Cr (VI) kinetic adsorption of Cr (VI) by banana peel dust adjusted to the pseudo-first order model.

Table 7. Adjustment parameter of Cr (VI) adsorption data to the evaluated kinetic models.

Model	Equation	Parameter	YP	PF	CP	CH	CR
Pseudo-first order	$q_t = q_e(1 - e^{-k_1 t})$	q_{e1} (mg/g)	21.702 ± 1	30.298 ± 0.015	9.634 ± 1	14.46 ± 0.765	16.663 ± 0.5
		k_1 (min^{-1})	83.231	6.366 ± 2.248	1.046 ± 0.85	49.0591	3877.719
		R^2	0.812	0.999	0.995	0.783	0.807
		Reduced Chi-Square	10.987	0.0021	0.04	5.861	4.442
		σ^2	0.736	0.038	0.045	0.893	0.757
Pseudo-second order	$q_t = \dfrac{t}{\left(\frac{1}{q_e^2 k_2}\right) + \left(\frac{t}{q_e}\right)}$	q_{e2} (mg/g)	21.702 ± 1	30.339	9.6673 ± 0.073	11.508 ± 1.43	16.663 ± 0.54
		k_2 (g/mg.min)	6.015	2.977 ± 1.29	0.896 ± 0.904	8.749 ± 1.437	2.437×10^{19}
		R^2	0.812	0.999	0.996	0.999	0.807
		Reduced Chi-Square	10.987	7.116×10^{-4}	0.039	15.544	4.442
		σ^2	0.736	0.0005	0.041	0.004	0.747
Elovich	$q_t = \frac{1}{\beta}\ln(\alpha\beta) + \frac{1}{\beta}\ln(t)$	β (g/mg)	0.504 ± 2.157	3.579	7.633 ± 2.157	0.698 ± 0.061	0.596 ± 0.05
		α (mg/g min)	$1.242.464 \pm 8$	4.248×10^{44}	1.205×10^{29}	389.198 ± 31	212.943 ± 17
		R^2	0.992	0.998	0.997	0.986	0.979
		Reduced Chi-Square	0.448	0.185	0.033	0.377	0.482
		σ^2	0.049	0.040	0.041	0.053	0.068
Intraparticle diffusion	$q_t = k_3 t^{0.5}$	k_3	1.178	1.500	0.481	0.788	0.925
		R^2	1.433	3.159	3.027	1.317	0.951
		Reduced Chi-Square	128.225	347.792	34.095	56.252	41.939
		σ^2	15.873	10.987	10.746	15.946	17.457

The experimental kinetic data of Cr (VI) removal of the five evaluated bioadsorbents were fitted to the pseudo-second order model, as shown in Figure 11. The data in Table 7 and the plot indicate that the model accurately describes the kinetic behavior of PF, CP, and CH. This suggests that the rate of adsorption of chromium (VI) at the adsorbent surface is principally controlled by the chemical exchanges between the metal and the binding sites on the adsorbent [61], as well as the strength of these interactions [62]. Consequently, as time progresses, the number of active sites on the adsorbent surface decreases, resulting in a decrease in the rate of adsorption [63]. This adjustment also suggests that the rate of adsorption eventually becomes negligible when the concentration of metal ions in the solution approaches zero, indicating that the process reaches equilibrium. The magnitude of the equilibrium constant (k_2) suggests that the rate of adsorption follows this order CH > PF > CP. Furthermore, the calculated q_e values align with the experimental results when using the pseudo-second order kinetic model. Similar data were found when using sawdust modified with formaldehyde [64] and *Luffa cylindrica* activated carbon [65].

Elovich's kinetic model is another widely used model for describing the adsorption kinetics of heavy metal ions by adsorbents, including chromium (VI). In this model, the rate of adsorption is assumed to be limited by the number of active sites available on the adsorbent surface, as well as the surface coverage of adsorbed metal ions [66]. Based on the data presented in Table 7 and Figure 12, it can be inferred that the Elovich model provides a good fit for describing the kinetics of Cr (VI) adsorption by the five bioadsorbents evaluated. The results suggest that the disposal of active sites and the surface coverage of adsorbed metal ions are the primary factors that control the adsorption process. Additionally, the rate of adsorption is influenced by both the availability of active sites on the adsorbent surface and the strength of the chemical interactions between the metal ions and the adsorbent [67]. In the first stages of the process, a high number of active sites are available, resulting in rapid adsorption of metal ions. As the adsorption process continues, the availability of active sites decreases, leading to a decrease in the rate of adsorption. The constant β in the Elovich model represents the initial rate of adsorption, while the constant α is the extent of

surface coverage of adsorbed metal ions. Similar results were found when using rice husk ash [67] and pea peel activated carbon modified with $ZnCl_2$ [68].

The ID kinetic model is another widely used model for describing the adsorption kinetics of heavy metal ions by adsorbents, including chromium (VI). In this model, the kinetics of adsorption are assumed to be controlled by the diffusion of metal to the interior of the adsorbent particles [69]. Figure 13 and Table 7 give evidence that the adsorption kinetics of Cr (VI) of the five evaluated bioadsorbents is not described by the intraparticle diffusion model, suggesting that the rate of adsorption is not controlled by the diffusion of metal ions from the bulk solution into the interior of the adsorbent particles. These results are consistent with those reported by Pabithra et al. [70], where the metal adsorption process is non-linear, and the intra-particle diffusion model did not provide evidence of the metal ion adsorption mechanism.

The experimental kinetic data show good fitting using the pseudo-second order, pseudo-first order, and Elovich models, indicating that the adsorption is mainly controlled by chemisorption. This implies that there is an exchange of Cr (VI) cations with the functional groups present on the biomass surface, such as COO^- and OH groups of cellulose and hemicellulose [71]. The reason for this is the creation of chemical bonds between the adsorbent and the adsorbate at the surface [72].

3.6. Equilibrium Analysis: Adsorption Isotherms

In Figure 14, the equilibrium adsorption of the ion concentration in water and adsorbent material is presented after 24 h of contact time at 30 °C. The adsorption isotherms are fitted to various models, including Langmuir, Freundlich, Redlich–Peterson, Temkin, and Sips models, which are shown in the figure.

The Langmuir isotherm model is frequently employed to analyze the adsorption characteristics of heavy metal ions, such as chromium (VI), by adsorbents. The model is based on the assumption that the surface of the solid features a finite amount of identical sites, and the adsorption of metal ions at these sites follows a monolayer coverage mechanism [73]. Based on Table 8, it can be inferred that the equilibrium adsorption data of Cr (VI) in YP, CP, and PF are well-described by the Langmuir model, indicating that the adsorption occurs through a monolayer coverage mechanism and the bioadsorbent surface possesses a finite number of identical sites for the adsorption of metal ions [74]. The maximum adsorption capacity, q_{max}, indicates the maximum amount of metal ions that can be adsorbed by the adsorbent surface under ideal conditions when all the available adsorption sites are occupied by metal ions; the obtained q_{max} for each adsorbent follows this order: CH > PF > CP > YP. The Langmuir constant K_L represents the affinity of the adsorbent for the metal ions and is related to the energy of adsorption [75], having YP with the highest affinity with the ion. The R_L parameter is the separation factor and indicates the reversibility ($R_L = 0$), favourability ($0 < R_L < 1$), linearity ($R_L = 1$), and unfavorability ($R_L > 1$) of the adsorption process; from the found values for this parameter, it can be said that the Cr (VI) adsorption by the evaluated adsorbents is favourable.

From the data in Table 8, it can be suggested that the Cr (VI) adsorption by YP occurs on a heterogeneous surface with a distribution of active sites and that the adsorption capacity varies with the surface coverage, considering the good adjustment to the Freundlich's isotherm model [76]. In addition, the adsorption capacity varies with the surface coverage. The value of n > 1 suggests that the intensity of adsorption is high and is affected by the initial concentration of the heavy metal [77].

Table 8. Fitting parameters of Cr (VI) adsorption by YP, PF, CP, CH, and CR to isotherm models.

Model	Equation	Parameter	YP	PF	CP	CH	CR
Freundlich	$q_e = K_F C_e^{1/n}$	K_F	8.631 ± 0.833	10.244 ± 2.453	12.428 ± 2.977	2.949 ± 1.172	0.376 ± 0.226
		n	2.216 ± 0.222	1.949 ± 0.397	2.372 ± 0.581	1.096 ± 0.22	0.681 ± 0.10
		R^2	0.977	0.892	0.836	0.878	0.935
		Reduced Chi-Square	1.899	21.825	32.457	10.152	7.149
		σ^2	0.893	7.456	6.898	7.464	7.149
Sips	$q_e = \frac{q_{ms} K_s C_e^{ms}}{1 + K_s C_e^{ms}}$	q_{ms}	36.842 ± 5.355	56.879 ± 10.127	52.819 ± 7.282	138.936 ± 8.321	36.123
		K_s	0.203 ± 0.074	0.158 ± 0.064	0.201 ± 0.067	0.021	9.94×10^{-5}
		m_s	0.456	0.398	0.451	0.476	3.573
		R^2	0.955	0.936	0.943	0.891	0.977
		Reduced Chi-Square	4.533	17.340	15.037	11.411	1.565
		σ^2	6.654	16.456	19.456	20.456	1.877
Langmuir	$q_e = \frac{(Q_{max} K_L C_e)}{1 + K_L C_e}$	q_{max}	38.842 ± 4.789	56.879 ± 8.769	52.819 ± 6.306	138.936 ± 6.650	240,948.7
		K_L	0.203 ± 0.066	0.159 ± 0.055	0.202 ± 0.058	0.021 ± 0.029	5.65×10^{-6}
		R_L	0.047	0.059	0.047	0.323	0.999
		R^2	0.955	0.936	0.943	0.890	0.003
		Reduced Chi-Square	3.626	13.005	11.278	9.129	
		σ^2	5.456	10.664	7.56	21.054	16.076
Redlich – Peterson	$q_e = \frac{(A C_e)}{1 + B C_e^g}$	A	$278,317.865 \pm 2.737$	6.759 ± 2.172	7.045 ± 0.854	2.663 ± 0.206	1.477
		B	$32,244.602 \pm 3.18$	0.019 ± 0.067	0.018 ± 0.019	5.099 ± 1.390	0.087
		g	0.549	1.631 ± 1.124	1.644 ± 0.293	12.497	0
		R^2	0.977	0.949	0.986	0.948	0.853
		Reduced Chi-Square	2.374	13.655	3.821	5.395	20.093
		σ^2	13.054	10.456	0.456	0.898	10.046
Temkin	$q_e = \frac{RT}{b_T} \ln(A_T C_e)$	A_T	8.999 ± 5.659	1.261 ± 0.287	1.564 ± 0.429	0.445 ± 0.051	198.549
		b_T	492.759 ± 83.969	183.041 ± 20.771	198.486 ± 25.191	153.057 ± 15.609	144.926
		B	5.115	13.769	12.698	16.467	17.399
		R^2	0.874	0.951	0.940	0.951	0.988
		Reduced Chi-Square	10.175	9.864	11.869	4.087	
		σ^2	25.056	6.456	10.456	12.465	20.091

The Temkin model assumes that the process involves a reduction in the adsorption energy as the surface coverage increases due to the interactions between the adsorbate and the adsorbent surface [78]. Good fitting between the experimental results of Cr (VI) by PF, CP, CH, and CR and the Temkin isotherm model suggests that the adsorption involves a decrease in the adsorption energy as the surface coverage increases, due to the interactions between the adsorbate and the adsorbent surface [79]. The Temkin constant A is related to the heat of adsorption, which represents the energy released or absorbed during the adsorption process following the order CR > CP > PF > CH. The Temkin constant B is related to the adsorption energy, which indicates the strength of the interactions between the adsorbate and the adsorbent surface, having CR and CH the strongest interaction with the adsorbate, which could enhance the retention of the metal in the structure of the adsorbent and it could be easily immobilized by carbonization or in concrete [80], for example.

The Sips model described the adsorption of Cr (VI) by YP, PF, CP, and CR, suggesting that the adsorption occurs through multilayer adsorption on a heterogeneous surface and that the adsorbent surface contains varying degrees of affinity for the metal ions [81]. The values of the maximum adsorption capacity (q_{ms}) are similar to the Langmuir model's

results, which is common, taking into account that the structure of both equations is alike, considering the Sips model, the heterogeneity of the adsorbent surface across the m_s parameter. The Redlich–Petersen isotherm model fitted the equilibrium adsorption of Cr (VI) by YP, PF, CP, and CH, suggesting that the adsorption of the adsorbate occurs through a combination of monolayer and multilayer adsorption mechanisms, and the adsorption sites on the adsorbent surface have a distribution of energies [82].

Table 9 compares the results obtained in previous studies that use lignocellulosic-based adsorbents for the removal of Cr (VI). The table shows that when the pH was not acidic, the adsorption capacity decreased. This is because at low pH levels, the surface of the adsorbents becomes protonated, and the existing chromium species are anions such as chromates and dichromates. These anions can be easily attached to the adsorbent due to electrostatic forces [40].

Table 9. Maximum adsorption capacity comparison of different adsorbent materials.

Biomass	Better Adjustment Model	Langmuir's qmax (mg/g)	Reference
Activated carbon prepared from apple peels	Freundlich	36.01	[83]
Wheat bran		4.2	
Wheat bran calcinated at 500 °C	Freundlich	7.6	[14]
Wheat bran calcinated at 1000 °C		29.3	
Sawdust modified with formaldehyde	Freundlich	8.84	[64]
Luffa cylindrica activated carbon	Freundlich	188.5	[65]
Rice husk ash	Temkin and Dubinin-Radushkevich	4.1	[67]
Pea peel activated carbon modified with ZnCl$_2$	Langmuir, Freundlich and Temkin	306.75	[68]
Banana peel dust	Langmuir	20.46	[60]
Yam peel	Langmuir, Freundlich, Sips and Redlich–Peterson	38.842	
Palm fibrillates	Langmuir, Temkin, Sips and Redlich–Peterson	56.879	This study
Cassava peel		52.819	
Cocoa husk	Redlich–Peterson and Temkin	138.936	
Corn residues	Freundlich, Sips, Langmuir y Temkin	240,948.7	

3.7. Future Approach and Practical Applications

Lignocellulosic adsorbents have shown great potential for the removal of contaminants from water due to their low cost, availability, and eco-friendliness [84]. Although bioadsorption is a technology studied in different countries, it still is in its developing phases, and efforts are needed to improve its performance and cost-effectiveness, considering its advantages over conventional adsorbents. The use of bioadsorbents for removing heavy metals has been a topic of great interest due to the rising demand for high-quality water. This demand has prompted researchers to focus on wastewater recovery and reuse, as well as the recovery of the ion and the final disposition of the exhausted adsorbent at the end of its useful life [85].

Industrial wastewater contains a wide range of organic and inorganic pollutants that can have a significant impact on water quality. Although the use of biosorbents for heavy metal removal has been studied extensively, there is still much to explore in terms of addressing the complex challenges presented by industrial wastewater. This represents a promising opportunity for researchers to develop new and effective solutions to the problem of heavy metal contamination [86]. In addition, there is a need to explore not only the reusability of adsorbents through cycles of adsorption–desorption, but also to determine how they are affected by microorganisms, which are also present in wastewater, due to the risk of releasing the contaminants retained in their lignocellulosic matrix. Based on these findings, actions must be taken to increase their lifespan against pathogenic agents

and find suitable techniques for immobilizing and stabilizing the remaining contaminants retained in the biomass.

While small-scale studies have shown that biosorbents can be effective and practical for removing heavy metals, their applicability in the field may be limited. Pilot studies and field implementation are crucial for understanding the performance and potential performances of different biosorbents. While many laboratory experiments have been conducted on biosorption technology, implementation remains a challenge due to the need to assess the behavior of the process under dynamic conditions, which differ from those of batch systems. In this sense, from a phenomenological point of view, there is a big gap in the research field, and this could lead to the development of a standardized model for the kinetic and adsorption rates in the equilibrium conditions for water–solid systems, considering the models used until today are based on gas–solid interactions.

For scaling up the adsorption process, the use of Computed Aided Process Engineering (CAPE) as a tool for studying the effect of difficult-to-determine variables, such as mass transfer coefficients, on the process in packed bed systems, simulation in software such as Aspen adsorption can be used to design processes and find behaviors that approach reality, especially when there is not much budget for experimental research before building the prototype equipment. The above, considering the scale-up of the process, is necessary to make it applicable for large-scale water treatment. Further research is needed to study the feasibility and cost-effectiveness of the scale-up process using computational tools and analysis under economic, exergy, and environmental parameters in order to establish sustainability from an integral perspective [87].

There is a growing effort to explore novel materials, enhance the efficacy of current biosorbents, and develop hybrid technologies that target multicomponent biosorption, incorporating methods such as electrocoagulation [88], ozonation [89], and photocatalysis [90] as a second phase for degrading the pollutants. Research efforts are also underway to explore the potential of hybrid biosorbents derived from a variety of agricultural waste materials. In addition, the use of nanocomposites is emerging as a promising approach for the efficient removal of toxic pollutants and heavy metals from aqueous solutions, although there is still a considerable distance to cover before reaching on-site applications. Biosorbents are considered eco-friendly, biodegradable, and cost-effective adsorbents, representing a smart technology concept that continues to evolve in response to growing demands.

4. Conclusions

This study evaluates five dried lignocellulosic bioadsorbents prepared from corn waste, palm fiber, and the peels of yam, cassava, and cocoa for removing Cr (VI) from a synthetic aqueous solution. The SEM-EDS analysis revealed that the predominant elements in the structure of the bioadsorbents were carbon and oxygen, and the mechanism might be controlled by the incorporation of Cr (VI) into the structure of the biomaterials. The adsorption efficiencies of the metal were strongly dependent on pH and adsorbent dosage. The maximal adsorption efficiency of 99.11% was obtained at pH 2, bioadsorbent dose of 0.03 mg, 30 °C, and 0.5 mm of particle size. Adsorption equilibrium data fitted well in the Redlich–Peterson and Temkin models (R^2 = 0.95), indicating that the phenomenon occurs in a multilayer. Pseudo-second order and Elovich kinetic models adjusted the kinetics of chromium (VI) at the evaluated conditions. The assessed maximum adsorption capacities were 38.84, 56.88, 52.82, 138.94, and 240,948.7 mg/g for YP, PF, CP, CH, and CR, respectively. The results demonstrated that the evaluated lignocellulosic bioadsorbents could be utilized as an economical and environmentally benign adsorbent at a low cost, and the combination with other technologies would allow for the diminution of the concentration of Cr (VI) in the treated waters more efficiently.

References

1. Prasad, S.; Yadav, K.K.; Kumar, S.; Gupta, N.; Cabral-Pinto, M.M.S.; Rezania, S.; Radwan, N.; Alam, J. Chromium contamination and effect on environmental health and its remediation: A sustainable approaches. *J. Environ. Manag.* **2021**, *285*, 112174. [CrossRef]
2. Vaicelyte, A.; Janssen, C.; Le Borgne, M.; Grosgogeat, B. Cobalt–Chromium Dental Alloys: Metal Exposures, Toxicological Risks, CMR Classification, and EU Regulatory Framework. *Crystals* **2020**, *10*, 1151. [CrossRef]
3. Butler, L.; Lall, U.; Bonnafous, L. Cumulative Heavy Metal Contamination in Mining Areas of the Rimac, Peru Basin. 2017, pp. 1–27. Available online: http://water.columbia.edu/files/2018/01/13.2017.Butler.Draft_.Cumulative-heavy-metal-contamination-in-mining-areas.pdf (accessed on 20 February 2023).
4. Ratnalu, G.V.; Dhakate, R. Human health hazard evaluation with reference to chromium (Cr+3 and Cr+6) in groundwater of Bengaluru Metropolitan City, South India. *Arab. J. Geosci.* **2021**, *14*, 1–19. [CrossRef]
5. Tumolo, M.; Ancona, V.; De Paola, D.; Losacco, D.; Campanale, C.; Massarelli, C.; Uricchio, V.F. Chromium Pollution in European Water, Sources, Health Risk, and Remediation Strategies: An Overview. *Int. J. Environ. Res. Public Health* **2020**, *17*, 5438. [CrossRef] [PubMed]
6. Wise, J.P.; Young, J.L.; Cai, J.; Cai, L. Current understanding of hexavalent chromium [Cr(VI)] neurotoxicity and new perspectives. *Environ. Int.* **2022**, *158*, 106877. [CrossRef]
7. Sharma, P.; Singh, S.P.; Parakh, S.K.; Tong, Y.W. Health hazards of hexavalent chromium (Cr (VI)) and its microbial reduction. *Bioeng.* **2022**, *13*, 4923–4938. [CrossRef]
8. Xu, C.; He, S.; Liu, Y.; Zhang, W.; Lu, D. Bioadsorption and biostabilization of cadmium by Enterobacter cloacae. *Chemosphere* **2017**, *173*, 622–629. [CrossRef]
9. Patriota, S.N.; Francisco, W.; Araújo, D.F.; Mulholland, D.S. Adsorption of Copper and Methylene Blue on an Agrowaste of Mauritia Flexuosa. *J. Environ. Eng.* **2020**, *146*, 04020039. [CrossRef]
10. Khalil, U.; Shakoor, M.B.; Ali, S.; Ahmad, S.R.; Rizwan, M.; Alsahli, A.A.; Alyemeni, M.N. Selective removal of hexavalent chromium from wastewater by rice husk: Kinetic, isotherm and spectroscopic investigation. *Water* **2021**, *13*, 263. [CrossRef]
11. Haroon, H.; Ashfaq, T.; Gardazi, S.M.H.; Sherazi, T.A.; Ali, M.; Rashid, N.; Bilal, M. Equilibrium kinetic and thermodynamic studies of Cr(VI) adsorption onto a novel adsorbent of Eucalyptus camaldulensis waste: Batch and column reactors. *Korean J. Chem. Eng.* **2016**, *33*, 2898–2907. [CrossRef]
12. Zhao, J.; Shen, X.-J.; Domene, X.; Alcañiz, J.-M.; Liao, X.; Palet, C. Comparison of biochars derived from different types of feedstock and their potential for heavy metal removal in multiple-metal solutions. *Sci. Rep.* **2019**, *9*, 9869. [CrossRef] [PubMed]
13. Mullick, A.; Moulik, S.; Bhattacharjee, S. Removal of Hexavalent Chromium from Aqueous Solutions by Low-Cost Rice Husk-Based Activated Carbon: Kinetic and Thermodynamic Studies. *Indian Chem. Eng.* **2018**, *60*, 58–71. [CrossRef]

14. Ogata, F.; Nagai, N.; Itami, R.; Nakamura, T.; Kawasaki, N. Potential of virgin and calcined wheat bran biomass for the removal of chromium(VI) ion from a synthetic aqueous solution. *J. Environ. Chem. Eng.* **2020**, *8*, 103710. [CrossRef]

15. Sivakumar, D.; Shankar, D.; Mahalakshmi, R.; Deepalakshmi, K. Kinetic Model Studies on Removal of Hexavalent Chromium-Sugarcane Bagasse Powder. *Int. Res. J. Multidiscip. Sci. Technol.* **2017**, *2*, 37–43.

16. Chen, S.; Yue, Q.; Gao, B.; Li, Q.; Xu, X.; Fu, K. Adsorption of hexavalent chromium from aqueous solution by modified corn stalk: A fixed-bed column study. *Bioresour. Technol.* **2012**, *113*, 114–120. [CrossRef] [PubMed]

17. Thakur, V.; Sharma, E.; Guleria, A.; Sangar, S.; Singh, K. Modification and management of lignocellulosic waste as an ecofriendly biosorbent for the application of heavy metal ions sorption. *Mater. Today Proc.* **2020**, *32*, 608–619. [CrossRef]

18. Benhabiles, S.; Rida, K. Production of efficient activated carbon from sawdust for the removal of dyes in single and binary systems–a full factorial design. *Part. Sci. Technol.* **2021**, *39*, 237–251. [CrossRef]

19. Moreno Sader, K.; León Pulido, J.; González-Delgado, Á. Evaluation of dual crude palm and kernel oil production in North Colombia via computer-aided exergy analysis. *Rev. ION* **2021**, *34*, 31–41. [CrossRef]

20. *D1687-17*; Standard Test Methods for Chromium in Water. ASTM: West Conshohocken, PA, USA, 2017. [CrossRef]

21. Mahmood-Ul-Hassan, M.; Yasin, M.; Yousra, M.; Ahmad, R.; Sarwar, S. Kinetics, isotherms, and thermodynamic studies of lead, chromium, and cadmium bio-adsorption from aqueous solution onto Picea smithiana sawdust. *Environ. Sci. Pollut. Res.* **2018**, *25*, 12570–12578. [CrossRef]

22. Sereshti, H.; Zamiri Afsharian, E.; Esmaeili Bidhendi, M.; Rashidi Nodeh, H.; Afzal Kamboh, M.; Yilmaz, M. Removal of phosphate and nitrate ions aqueous using strontium magnetic graphene oxide nanocomposite: Isotherms, kinetics, and thermodynamics studies. *Environ. Prog. Sustain. Energy* **2020**, *39*, e13332. [CrossRef]

23. Alhogbi, B.G. Potential of coffee husk biomass waste for the adsorption of Pb(II) ion from aqueous solutions. *Sustain. Chem. Pharm.* **2017**, *6*, 21–25. [CrossRef]

24. Panda, G.C.; Das, S.K.; Bandopadhyay, T.S.; Guha, A.K. Adsorption of nickel on husk of Lathyrus sativus: Behavior and binding mechanism. *Colloids Surf. B Biointerfaces* **2007**, *57*, 135–142. [CrossRef] [PubMed]

25. Briat, J.F.; Dubos, C.; Gaymard, F. Iron nutrition, biomass production, and plant product quality. *Trends Plant Sci.* **2015**, *20*, 33–40. [CrossRef] [PubMed]

26. Hawkesford, M.J.; Barraclough, P. *The Molecular and Physiological Basis of Nutrient Use Efficiency in Crops*; Wiley-Blackwell: Hoboken, NJ, USA, 2011. [CrossRef]

27. Tejada-Tovar, C.; Villabona-Ortíz, A.; Ruiz-Paternina, E.; Herrera-Barros, A.; Ortega-Toro, R. Characterization and use of agroindustrial by-products in the removal of metal ions in aqueous solution. *J. Teknol.* **2019**, *81*, 151–158. [CrossRef]

28. Tejada-Tovar, C.; Villabona-Ortíz, A.; Gonzalez-Delgado, Á.; Granados-Conde, C.; Jimenez-Villadiego, M. Kinetics of Mercury and Nickel Adsorption Using Chemically Pretreated Cocoa (*Theobroma cacao*) Husks. *Trans. ASABE* **2019**, *62*, 461–466. [CrossRef]

29. Tejada-Tovar, C.; Herrera-Barros, A.; Villabona-Ortíz, A. Assessment of Chemically Modified Lignocellulose Waste for the Adsorption of Cr (VI). *Rev. Fac. Ing.* **2020**, *29*, e10298. [CrossRef]

30. Chen, Y.; An, D.; Sun, S.; Gao, J.; Qian, L. Reduction and Removal of Chromium VI in Water by Powdered Activated Carbon. *Materials* **2018**, *11*, 269. [CrossRef] [PubMed]

31. Xia, L.; Xu, X.; Zhu, W.; Huang, Q.; Chen, W. A comparative study on the biosorption of Cd2+ onto Paecilomyces lilacinus XLA and Mucoromycote sp. XLC. *Int. J. Mol. Sci.* **2015**, *16*, 15670–15687. [CrossRef] [PubMed]

32. Okoli, C.P.; Diagboya, P.N.; Anigbogu, I.O.; Olu-Owolabi, B.I.; Adebowale, K.O. Competitive biosorption of Pb(II) and Cd(II) ions from aqueous solutions using chemically modified moss biomass (*Barbula lambarenensis*). *Environ. Earth Sci.* **2017**, *76*, 1–10. [CrossRef]

33. Al-Ghouti, M.A.; Al-Absi, R.S. Mechanistic understanding of the adsorption and thermodynamic aspects of cationic methylene blue dye onto cellulosic olive stones biomass from wastewater. *Sci. Rep.* **2020**, *10*, 15928. [CrossRef]

34. Tang, J.; Li, Y.; Wang, X.; Daroch, M. Effective adsorption of aqueous Pb2+ by dried biomass of Landoltia punctata and Spirodela polyrhiza. *J. Clean. Prod.* **2017**, *145*, 25–34. [CrossRef]

35. Lara, J.; Tejada, C.; Villabona, Á.; Arrieta, A.; Conde, C.G. Adsorción de plomo y cadmio en sistema continuo de lecho fijo sobre residuos de cacao. *Rev. Ion* **2016**, *29*, 113–124. [CrossRef]

36. Vizcaíno Mendoza, L.; Fuentes Molina, N.; González Fragozo, H. Adsorption of lead (II) with stems and and leaves of Eichhornia crassipes in aqueous solution. *Rev. UDCA Actual. Divulg. Científica* **2017**, *20*, 435–444. [CrossRef]

37. Fernández-Maestre, R.; Colpas-Castillo, F. Mercury and cadmium adsorption in subbituminous xanthated, sulfonated or activated carbon and commercial synthetic resin. *Rev. UDCA Actual. Divulg. Científica* **2015**, *18*, 241–250. [CrossRef]

38. Wang, S.; Kwak, J.H.; Islam, M.S.; Naeth, M.A.; Gamal El-Din, M.; Chang, S.X. Biochar surface complexation and Ni(II), Cu(II), and Cd(II) adsorption in aqueous solutions depend on feedstock type. *Sci. Total Environ.* **2020**, *712*, 136538. [CrossRef] [PubMed]

39. Hedberg, J.; Fransson, K.; Prideaux, S.; Roos, S.; Jönsson, C.; Wallinder, I.O. Improving the Life Cycle Impact Assessment of Metal Ecotoxicity: Importance of Chromium Speciation, Water Chemistry, and Metal Release. *Sustainability* **2019**, *11*, 1655. [CrossRef]

40. Mädler, S.; Sun, F.; Tat, C.; Sudakova, N.; Drouin, P.; Tooley, R.J.; Reiner, E.J.; Switzer, T.A.; Dyer, R.; Kingston, H.M.S.; et al. Trace-Level Analysis of Hexavalent Chromium in Lake Sediment Samples Using Ion Chromatography Tandem Mass Spectrometry. *J. Environ. Prot.* **2016**, *7*, 422–434. [CrossRef]

41. Genawi, N.M.; Ibrahim, M.H.; El-Naas, M.H.; Alshaik, A.E. Chromium Removal from Tannery Wastewater by Electrocoagulation: Optimization and Sludge Characterization. *Water* **2020**, *12*, 1374. [CrossRef]

42. Sivagami, K.; Sakthivel, K.P.; Nambi, I.M. Advanced oxidation processes for the treatment of tannery wastewater. *J. Environ. Chem. Eng.* **2018**, *6*, 3656–3663. [CrossRef]

43. Dobrosz-Gómez, I.; Gómez, M.; Santa, C. Optimización del Proceso de Adsorción de Cr (VI) sobre Carbón Activado de Origen Bituminoso. *Inf. Tecnol.* **2018**, *29*, 43–56. [CrossRef]

44. Bhatti, I.A.; Ahmad, N.; Iqbal, N.; Zahid, M.; Iqbal, M. Chromium adsorption using waste tire and conditions optimization by response surface methodology. *J. Environ. Chem. Eng.* **2017**, *5*, 2740–2751. [CrossRef]

45. Ben Khalifa, E.; Rzig, B.; Chakroun, R.; Nouagui, H.; Hamrouni, B. Application of response surface methodology for chromium removal by adsorption on low-cost biosorbent. *Chemom. Intell. Lab. Syst.* **2019**, *189*, 18–26. [CrossRef]

46. Vyavahare, G.D.; Gurav, R.G.; Jadhav, P.P.; Patil, R.R.; Aware, C.B.; Jadhav, J.P. Response surface methodology optimization for sorption of malachite green dye on sugarcane bagasse biochar and evaluating the residual dye for phyto and cytogenotoxicity. *Chemosphere* **2018**, *194*, 306–315. [CrossRef] [PubMed]

47. Tran, H.N.; You, S.J.; Chao, H.P. Thermodynamic parameters of cadmium adsorption onto orange peel calculated from various methods: A comparison study. *J. Environ. Chem. Eng.* **2016**, *4*, 2671–2682. [CrossRef]

48. Wang, H.; Chu, Y.; Fang, C.; Huang, F.; Song, Y.; Xue, X. Sorption of tetracycline on biochar derived from rice straw under different temperatures. *PLoS ONE* **2017**, *12*, e0182776. [CrossRef]

49. Krika, F.; Azzouz, N.; Ncibi, M.C. Adsorptive removal of cadmium from aqueous solution by cork biomass: Equilibrium, dynamic and thermodynamic studies. *Arab. J. Chem.* **2016**, *9*, S1077–S1083. [CrossRef]

50. Hadavifar, M.; Bahramifar, N.; Younesi, H.; Li, Q. Adsorption of mercury ions from synthetic and real wastewater aqueous solution by functionalized multi-walled carbon nanotube with both amino and thiolated groups. *Chem. Eng. J.* **2014**, *237*, 217–228. [CrossRef]

51. Hernández Rodriguez, M.; Yperman, J.; Carleer, R.; Maggen, J.; Daddi, D.; Gryglewicz, G.; Van der Bruggen, B.; Falcón Hernández, J.; Otero Calvis, A. Adsorption of Ni(II) on spent coffee and coffee husk based activated carbon. *J. Environ. Chem. Eng.* **2018**, *6*, 1161–1170. [CrossRef]

52. Naseem, K.; Huma, R.; Shahbaz, A.; Jamal, J.; Ur Rehman, M.Z.; Sharif, A.; Ahmed, E.; Begum, R.; Irfan, A.; Al-Sehemi, A.G.; et al. Extraction of Heavy Metals from Aqueous Medium by Husk Biomass: Adsorption Isotherm, Kinetic and Thermodynamic study. *Z. Phys. Chem.* **2019**, *233*, 201–223. [CrossRef]

53. Villabona-Ortiz, Á.; Tejada-Tovar, C.; Darío González-Delgado, Á.; Herrera-Barros, A.; Silvera-Charris, R. Removal of Cr(VI) ions from aqueous solution using orange peel residual biomass: Thermodynamic and sorption-desorption study. *Desalin. Water Treat.* **2020**, *203*, 309–314. [CrossRef]

54. Villabona-Ortíz, A.; Tejada-Tovar, C.; González-Delgado, Á.D.; Herrera-Barros, A.; Cantillo-Arroyo, G. Immobilization of Lead and Nickel Ions from Polluted Yam Peels Biomass Using Cement-Based Solidification/Stabilization Technique. *Int. J. Chem. Eng.* **2019**, *2019*, 5413960. [CrossRef]

55. Ndiba, P.; Axe, L.; Boonfueng, T. Heavy metal immobilization through phosphate and thermal treatment of dredged sediments. *Environ. Sci. Technol.* **2008**, *42*, 920–926. [CrossRef]

56. Guo, B.; Liu, B.; Yang, J.; Zhang, S. The mechanisms of heavy metal immobilization by cementitious material treatments and thermal treatments: A review. *J. Environ. Manag.* **2017**, *193*, 410–422. [CrossRef] [PubMed]

57. Zhou, Q.; Duan, Y.; Chen, M.; Liu, M.; Lu, P. Studies on Mercury Adsorption Species and Equilibrium on Activated Carbon Surface. *Energy Fuels* **2017**, *31*, 14211–14218. [CrossRef]

58. Danmallam, A.A.; Dabature, W.L.; Pindiga, N.Y.; Magaji, B.; Aboki, M.A.; Ibrahim, D.; Zanna, U.A.S.; Muktar, M.S. The Kinetics of the Adsorption Process of Cr (VI) in Aqueous Solution Using Neem Seed Husk (*Azadirachta indica*) Activated Carbon. *Phys. Sci. Int. J.* **2020**, *24*, 1–13. [CrossRef]

59. Saha, R.; Mukherjee, K.; Saha, I.; Ghosh, A.; Ghosh, S.K.; Saha, B. Removal of hexavalent chromium from water by adsorption on mosambi (*Citrus limetta*) peel. *Res. Chem. Intermed.* **2013**, *39*, 2245–2257. [CrossRef]

60. Mondal, N.K.; Samanta, A.; Chakraborty, S.; Shaikh, W.A. Enhanced chromium (VI) removal using banana peel dust: Isotherms, kinetics and thermodynamics study. *Sustain. Water Resour. Manag.* **2017**, *4*, 489–497. [CrossRef]

61. Hubbe, M.A.; Azizian, S.; Douven, S. Implications of apparent pseudo-second-order adsorption kinetics onto cellulosic materials: A review. *BioResources* **2019**, *14*, 7582–7626. [CrossRef]

62. Perez, T.; Pasquini, D.; De Faria Lima, A.; Rosa, E.V.; Sousa, M.H.; Cerqueira, D.A.; De Morais, L.C. Efficient removal of lead ions from water by magnetic nanosorbents based on manganese ferrite nanoparticles capped with thin layers of modified biopolymers. *J. Environ. Chem. Eng.* **2019**, *7*, 102892. [CrossRef]

63. Gómez-Aguilar, D.L.; Rodríguez-Miranda, J.P.; Esteban-Muñóz, J.A.; Betancur, J.F. Coffee Pulp: A Sustainable Alternative Removal of Cr (VI) in Wastewaters. *Processes* **2019**, *7*, 403. [CrossRef]

64. Chakraborty, R.; Verma, R.; Asthana, A.; Vidya, S.S.; Singh, A.K. Adsorption of hazardous chromium (VI) ions from aqueous solutions using modified sawdust: Kinetics, isotherm and thermodynamic modelling. *Int. J. Environ. Anal. Chem.* **2021**, *101*, 911–928. [CrossRef]

65. Nwosu-Obieogu, K.; Okolo, B.I. Biosorption of chromium (VI) from textile waste water using luffa cylindrica activated carbon. *Environ. Qual. Manag.* **2020**, *29*, 23–31. [CrossRef]

66. Bello, O.S.; Alao, O.C.; Alagbada, T.C.; Olatunde, A.M. Biosorption of ibuprofen using functionalized bean husks. *Sustain. Chem. Pharm.* **2019**, *13*, 100151. [CrossRef]

67.	Priya, A.K.; Yogeshwaran, V.; Rajendran, S.; Hoang, T.K.A.; Soto-Moscoso, M.; Ghfar, A.A.; Bathula, C. Investigation of mechanism of heavy metals (Cr^{6+}, Pb^{2+} & Zn^{2+}) adsorption from aqueous medium using rice husk ash: Kinetic and thermodynamic approach. *Chemosphere* **2022**, *286*, 131796. [CrossRef] [PubMed]

68.	Sahlabji, T.; El-Nemr, M.A.; El Nemr, A.; Ragab, S.; Alghamdi, M.M.; El-Zahhar, A.A.; Idris, A.M.; Said, T.O. High surface area microporous activated carbon from Pisum sativum peels for hexavalent chromium removal from aquatic environment. *Toxin Rev.* **2021**, *41*, 639–649. [CrossRef]

69.	Negm, N.A.; Abd, M.G.; Wahed, E.; Rahman, A.; Hassan, A.; Abou, M.T.H. Feasibility of metal adsorption using brown algae and fungi: Effect of biosorbents structure on adsorption isotherm and kinetics Feasibility of metal adsorption using brown algae and fungi: Effect of biosorbents structure on adsorption isotherm and kine. *J. Mol. Liq.* **2018**, *264*, 292–305. [CrossRef]

70.	Pavithra, S.; Thandapani, G.; Sugashini, S.; Sudha, P.N.; Alkhamis, H.H.; Alrefaei, A.F.; Almutairi, M.H. Batch adsorption studies on surface tailored chitosan/orange peel hydrogel composite for the removal of Cr(VI) and Cu(II) ions from synthetic wastewater. *Chemosphere* **2021**, *271*, 129415. [CrossRef]

71.	Wang, H.; Shen, H.; Shen, C.; Li, Y.; Ying, Z.; Duan, Y. Kinetics and Mechanism Study of Mercury Adsorption by Activated Carbon in Wet Oxy-Fuel Conditions. *Energy Fuels* **2019**, *33*, 1344–1353. [CrossRef]

72.	Doke, K.M.; Khan, E.M. Equilibrium, kinetic and diffusion mechanism of Cr (VI) adsorption onto activated carbon derived from wood apple shell. *Arab. J. Chem.* **2017**, *10* (Suppl. S1), S252–S260. [CrossRef]

73.	Foo, K.Y.; Hameed, B.H. Insights into the modeling of adsorption isotherm systems. *Chem. Eng. J.* **2010**, *156*, 2–10. [CrossRef]

74.	Chen, Y.; Wang, H.; Zhao, W.; Huang, S. Four different kinds of peels as adsorbents for the removal of Cd (II) from aqueous solution: Kinetics, isotherm and mechanism. *J. Taiwan Inst. Chem. Eng.* **2018**, *88*, 146–151. [CrossRef]

75.	Banerjee, M.; Basu, R.K.; Das, S.K. Cr(VI) adsorption by a green adsorbent walnut shell: Adsorption studies, regeneration studies, scale-up design and economic feasibility. *Process Saf. Environ. Prot.* **2018**, *116*, 693–702. [CrossRef]

76.	Rane, N.M.; Admane, S.V.; Sapkal, R.S. Adsorption of Hexavalent Chromium from Wastewater by Using Sweetlime and Lemon Peel Powder by Batch Studies. In *Waste Management and Resource Efficiency*; Springer: Singapore, 2019. [CrossRef]

77.	Amro, A.N.; Abhary, M.K.; Shaikh, M.M.; Ali, S. Removal of lead and cadmium ions from aqueous solution by adsorption on a low-cost Phragmites biomass. *Processes* **2019**, *7*, 406. [CrossRef]

78.	Chu, K.H. Revisiting the Temkin Isotherm: Dimensional Inconsistency and Approximate Forms. *Ind. Eng. Chem. Res.* **2021**, *60*, 13140–13147. [CrossRef]

79.	Aiyesanmi, A.F.; Adebayo, M.A.; Arowojobe, Y. Biosorption of Lead and Cadmium from Aqueous Solution in Single and Binary Systems Using Avocado Pear Exocarp: Effects of Competing Ions. *Anal. Lett.* **2020**, 1–18. [CrossRef]

80.	Zhang, S.; Zhao, Y.; Guo, Z.; Ding, H. Stabilization/solidification of hexavalent chromium containing tailings using low-carbon binders for cemented paste backfill. *J. Environ. Chem. Eng.* **2021**, *9*, 104738. [CrossRef]

81.	Lim, L.B.L.; Priyantha, N.; Lu, Y.C.; Mohamad Zaidi, N.A.H. Adsorption of heavy metal lead using Citrus grandis (Pomelo) leaves as low-cost adsorbent. *Desalin. Water Treat.* **2019**, *166*, 44–52. [CrossRef]

82.	Amaku, J.F.; Ngwu, C.M.; Nnaji, J.C.; Odoemelam, S.A.; Ifeanyi, U.B.; Okorie, H.C.; Zubairu, S.M. Adsorption of Cr(VI) onto Azadirachta indica stem bark extract modified dolerite composite adsorbent. *Int. J. Environ. Anal. Chem.* **2021**, 1–18. [CrossRef]

83.	Enniya, I.; Rghioui, L.; Jourani, A. Adsorption of hexavalent chromium in aqueous solution on activated carbon prepared from apple peels. *Sustain. Chem. Pharm.* **2018**, *7*, 9–16. [CrossRef]

84.	Onoja, E.; Chandren, S.; Abdul Razak, F.I.; Mahat, N.A.; Wahab, R.A. Oil Palm (Elaeis guineensis) Biomass in Malaysia: The Present and Future Prospects. *Waste Biomass Valorization* **2019**, *10*, 2099–2117. [CrossRef]

85.	Yaashikaa, P.R.; Kumar, P.S.; Saravanan, A.; Vo, D.V.N. Advances in biosorbents for removal of environmental pollutants: A review on pretreatment, removal mechanism and future outlook. *J. Hazard. Mater.* **2021**, *420*, 126596. [CrossRef] [PubMed]

86.	Elgarahy, A.M.; Elwakeel, K.Z.; Mohammad, S.H.; Elshoubaky, G.A. A critical review of biosorption of dyes, heavy metals and metalloids from wastewater as an efficient and green process. *Clean. Eng. Technol.* **2021**, *4*, 100209. [CrossRef]

87.	González-Delgado, Á.D.; Moreno-sader, K.A.; Martínez-Consuegra, J.D. *Biorrefinación Sostenible del Camarón: Desarrollos Desde la Ingeniería de Procesos Asistida por Computador*; Corporación Universitaria Minuto de Dios–UNIMINUTO: Bogotá, Colombia, 2022; ISBN 9789587635584. [CrossRef]

88.	Al-Qodah, Z.; Tawalbeh, M.; Al-Shannag, M.; Al-Anber, Z.; Bani-Melhem, K. Combined electrocoagulation processes as a novel approach for enhanced pollutants removal: A state-of-the-art review. *Sci. Total Environ.* **2020**, *744*, 140806. [CrossRef] [PubMed]

89.	Ren, M.; Wang, J.; Wang, Z.; Sun, S.; Qiu, J.; Shi, Y.; Wang, Z.J.; Xie, Y. Activated carbon adsorption coupled with ozonation regeneration for efficient removal of chlorobenzene. *J. Environ. Chem. Eng.* **2022**, *10*, 107319. [CrossRef]

90.	Zhang, L.; Ma, P.; Dai, L.; Bu, Z.; Li, X.; Yu, W.; Cao, Y.; Guan, J. Removal of pollutants via synergy of adsorption and photocatalysis over MXene-based nanocomposites. *Chem. Eng. J. Adv.* **2022**, *10*, 100285. [CrossRef]